Construction of the Ukrainian Carpathian Wedge from low-temperature thermochronology and tectono-stratigraphic analysis

Marion Roger[1], Arjan de Leeuw[1], Peter van der Beek[2], Laurent Husson[1], Edward R. Sobel[2], Johannes Glodny[3] and Matthias Bernet[1]

[1]Institut des Sciences de la Terre (ISTerre), Université Grenoble Alpes, CNRS, IRD, 38000 Grenoble, France
[2]Institut für Geowissenschaften, Universität Potsdam, 14476 Potsdam, Germany
[3]GFZ German Research Centre for Geosciences, Potsdam 14473, Germany

Correspondence to: Marion Roger (marion.roger@univ-grenoble-alpes.fr)

Abstract. The evolution of orogenic wedges can be determined through stratigraphic and thermochronological analysis. We used apatite fission-track (AFT) and apatite and zircon (U-Th-Sm)/He (AHe and ZHe) low-temperature thermochronology to assess the thermal evolution of the Ukrainian Carpathians, a prime example of an orogenic wedge forming in a retreating subduction zone setting. Whereas most of our AHe ages are reset by burial heating, eight out of ten of our AFT ages are partially reset, and none of the ZHe ages are reset. We inverse-modelled our thermochronology data to determine the time-temperature paths of six of the eight nappes composing the wedge. The models were integrated with burial diagrams derived from the stratigraphy of the individual nappes, which allowed us to distinguish sedimentary from tectonic burial. This analysis reveals that accretion of successive nappes and their subsequent exhumation mostly occurred sequentially, with an apparent increase in exhumation rate towards the external nappes. Following a phase of tectonic burial, the nappes were generally exhumed when a new nappe was accreted whereas, in one case, duplexing resulted in prolonged burial. An early orogenic wedge formed with the accretion of the innermost nappe at 34 Ma, leading to an increase in sediment supply to the remnant basin. Most of the other nappes were accreted between 28-18 Ma. Modelled exhumation of the outermost nappe started at 12 Ma, and was accompanied by out-of-sequence thrusting. The latter was linked to emplacement of the wedge onto the European platform and consequent slab detachment. The distribution of thermochronological ages across the wedge, showing non-reset ages in both the inner and outer part of the belt, suggests that the wedge was unable to reach dynamic equilibrium for a period long enough to fully reset all thermochronometers. Non-reset ZHe ages indicate that sediments in the inner part of the Carpathian embayment were mostly supplied by the Inner Carpathians, while sediments in the outer part of the basin were derived mostly from the Teisseyre-Tornquist Zone (TTZ) or the south-western margin of the East-European Platform. Our results suggest that during the accretionary phase, few sediments were recycled from the wedge to the foredeep. Most of the sediments derived from the Ukrainian Carpathian wedge were likely transported directly to the present pro- and retro- foreland basins.

1 Introduction

Thin-skinned fold-and-thrust belts result from the accretion, stacking and exhumation of sediments from pre-existing basins trapped in convergence zones. These basins frequently evolve from rifted passive margins to orogens (e.g., Stockmal et al., 1986) and their stratigraphy of these basins provides a record of convergence-zone dynamics and the onset of orogeny, in particular when the sedimentary record is combined with subsequent exhumation paths that can be retrieved from detrital zircon and apatite grains using low-temperature thermochronology (e.g., Merten et al., 2010; Fillon et al., 2013; Vacherat et al., 2014; Andreucci et al., 2015; Castelluccio et al., 2016).

Sediments in the antecedent basin are brought to depth by sedimentary burial and integrated into the wedge through nappe stacking processes in two steps. Sediment deposition in the basin may bury older deposits under several kilometers of overburden. Sediment accumulation is bound to accelerate as the orogenic belt propagates toward the basin, by a

combination of enhanced erosion of the growing wedge, the backstop and the forebulge area, and creation of accommodation space by flexure of the underlying plate (e.g., Simpson, 2006; Sinclair, 2012) and possible dynamic subsidence of the foreland (e.g., Husson et al., 2014; Flament et al., 2015). Tectonic nappe stacking integrates the pre-existing basin step-by-step into the growing wedge. When the frontal thrust propagates into the adjacent former basin, the latter becomes a nappe that overrides more external areas of the basin. Overthrusting of the basin by the orogenic wedge leads to tectonic burial in addition to initial sedimentary burial. As thrusting propagates outwards and the wedge evolves, the newly formed nappes are sequentially uplifted and exhumed. Syn-orogenic deposits that accumulate on the newly formed thrust sheet, i.e., wedge-top sediments, might also be progressively incorporated into the wedge and eventually buried. This process repeats until plate convergence stops (Davis et al., 1983; Dahlen et al., 1984; Konstantinovskaia and Malavieille, 2005; Hoth et al., 2007). Overthrusting of a nappe may entrain a phase of internal deformation in the orogenic wedge that causes rock- and surface uplift (Hoth et al., 2007; Sinclair and Naylor, 2012). Steady state in the wedge may potentially be reached if the tectonic influx of material into the wedge and the outflow through erosion balance one another, so that the elevation and width of the wedge remain constant (Willett et al. 1993).

In the Carpathian fold-and-thrust belt, the main driver of foreland-basin subsidence and frontal accretion is slab roll-back rather than plate convergence (e.g., Royden and Faccenna, 2015). The elevation and width of the wedge provide an insufficient load to have created the observed foreland basin, which suggests that the subducting slab primarily drove subsidence (Royden and Karner, 1984; Royden and Burchfiel, 1989; Royden, 1993; Krzywiec and Jochym, 1996, 1997). Foreland subsidence was enhanced by the reactivation of pre-orogenic normal faults during the Miocene (Krzywiec, 2001; Tărăpoancă et al., 2003; Oszczypko et al., 2006), probably also predominantly due to flexuring of the lithosphere through slab rollback.

Previous studies in the East and Southeast Romanian Carpathians have focused on the timing of nappe-stacking and exhumation of the wedge. Using low-temperature thermochronology to quantify the erosion pattern on both sides of the wedge, Sanders et al. (1999) concluded that the southeast Carpathians can be treated as a doubly-vergent critical wedge, where the back thrusts are covered by Neogene volcanic rocks and sediments that accumulated in the retro-foreland basin. Further studies, however, inferred that the doubly-vergent wedge concept cannot be directly applied to the Romanian East and Southeast Carpathians, and that this belt is a singly vergent wedge that evolved through forward propagation of deformation over the subducting plate followed by significant out-of-sequence thrusting (Matenco et al., 2010; Merten et al., 2010). In contrast, the Western Carpathians might correspond to a doubly vergent wedge as back thrusts are present and some involve basement blocks (Mazzoli et al., 2010; Castelluccio et al., 2016). These contrasting views imply that caution should be exerted when extrapolating interpretations of wedge dynamics along the Carpathian arc, because the characteristics of the downgoing plate change markedly along strike.

Convergence in the Carpathians was mostly oblique to the East European Platform (EEP), except in the Ukrainian Carpathians, where it occurred perpendicular to the margin. This makes the Ukrainian Carpathians a promising site to resolve wedge dynamics, as well as the kinematics and drivers of nappe stacking. The structure and timing of nappe accretion in the Ukrainian Carpathians was previously studied by Nakapelyuk et al. (2018), employing balanced cross sections and low-temperature thermochronology. Their study suggested very rapid convergence starting in the Miocene, when most of the nappes were accreted and subsequently exhumed (Fig. 1).

To better understand the dynamics of accretionary wedge formation during slab roll-back and to constrain sediment fluxes in this type of orogen, we study the accretion-collision and exhumation phases of the Ukrainian Carpathian wedge from the Oligocene onward using thermal-history modelling based on low-temperature thermochronology and stratigraphic analysis. In particular, we constrain the timing and amount of sedimentary and tectonic burial for each nappe, as well as its subsequent exhumation.

2 Geological context

The Carpathian belt is the result of the collision of the Tisza-Dacia and Alps-Carpathian-Pannonian (ALCAPA) micro-plates with the East European Platform (Csontos et al., 1992; Schmid et al., 2008). These two microplates jointly moved to the North from the Late Cretaceous (Santonian; ~84 Ma) to the Oligocene (~34 Ma). From then on, they moved northeast into the Carpathian embayment, a deep-water area of oceanic to thinned continental crust with intervening ridges formed during Tethyan rifting (Handy et al., 2015). Most of the microplates' motion was accommodated by roll-back of the subducting European oceanic crust and rifted continental margin. ALCAPA motion was also promoted by extrusion from the convergence zone of the Alps (Sperner et al., 2002). Nappe accretion into the outer Carpathian thin-skinned wedge started in the Oligocene (Sandulescu, 1975; Nemčok et al., 2006; Schmid et al., 2008). The age of the terminal frontal thrust of the Outer Carpathians, which can be used as a proxy for collision, becomes younger from northwest to southeast along the orogen (Nemčok et al., 2006). Oblique collision occurred in the northwest Carpathians from 17-15 Ma (Nemcok et al., 2006 and references therein). Subsequent subduction roll-back towards the east led to continued nappe accretion in front of the wedge, coincident with back-arc extension in the Pannonian Basin (Tari et al., 1992; Horváth and Cloetingh, 1996). This was followed by collision in the Ukrainian Carpathians at approximately 12 Ma (Gągała et al., 2012; Nakapelyukh et al., 2018), and in the Romanian Carpathians after 10 Ma (Matenco and Bertotti, 2000). The cessation of contraction in the belt has been linked to break-off of the European slab, which also propagated from northwest to southeast (Nemcok et al., 1998; Wortel and Spakman, 2000; Cloetingh et al., 2004; Handy et al., 2015). The slab is still attached in the south-easternmost corner of the Carpathians, known as the Vrancea Zone, where its pull on the overriding crust, in combination with the induced mantle flow, causes extremely rapid localised subsidence (Royden and Karner, 1984; Şengül-Uluocak et al., 2019). Whereas this sequence of events explains most observables, other models exist, for instance including successive panels of the slab breaking off, activating mantle cells and upwelling in the Pannonian Basin (Koněcný et al., 2002), or including lithosphere delamination and Neogene extension in the Pannonian realm leading to eastward extrusion of the Carpathian microplates by mantle flow (Kovács, 2012).

The Carpathians consist of an Inner and an Outer belt, separated by the Pieniny Klippen Belt (PKB). The inner Carpathians formed in the Cretaceous by thick-skinned stacking of nappes comprising the basement of the ALCAPA and Tisza-Dacia blocks and their Permian-Cretaceous sedimentary cover (Csontos and Vörös, 2004; Schmid et al., 2008). The Outer Carpathians are a thin-skinned accretionary prism, which developed from the Oligocene to the late Miocene, and which is composed of flysch nappes derived from the Carpathian embayment (Ślączka et al., 2005). In Ukraine, most of the thick-skinned Inner Carpathian units are covered by the Neogene volcanics that erupted on the edge of the Pannonian basin; they only crop out in a limited area next to the border with Romania. The PKB is the outermost unit of the Inner Carpathians outcropping in Ukraine. The PKB was thrust onto the Outer Carpathians (Fig. 1) during early to middle Miocene convergence (Castelluccio et al., 2016). Whether the PKB accommodated strike-slip motion and/or back-thrusting during the emplacement of the Inner Carpathians in Poland is debated (Ratschbacher et al., 1993; Nemčok et al., 2006; Castelluccio et al., 2016). The Ukrainian Carpathians mainly expose the outer flysch nappes of the belt (Fig. 1), which consist of a series of thin thrust sheets that contain Cretaceous to Miocene mostly deep-water clastic sediments. These outer nappes were accreted north-eastward and then thrust onto the East European Platform during the early to middle Miocene (Fig. 1c). Each nappe groups several units that display similar sedimentary sequences and share the same décollement horizon (Fig. 2). Convergence and accretion of the Carpathian wedge is thought to have started in the Oligocene in Ukraine, when the innermost nappes of the Outer Carpathians were integrated into the accretionary wedge (Gągała et al., 2012; Nakapelyukh et al., 2018).

Total convergence in the Ukrainian Carpathians is around 340 km, according to balanced cross-section restoration (Nakapelyukh et al., 2018). Low-temperature thermochronology data combined with balanced cross-sections have been interpreted to record two phases of shortening in Oligocene-Miocene times, as well as out-of-sequence thrusting in both the

Western and Eastern Carpathians (Matenco et al., 2010; Merten et al., 2010; Mazzoli et al., 2010; Castelluccio et al., 2016; Nakapelyukh et al., 2018). These studies postulate a slower convergence phase before the emplacement of the Outer Carpathian nappes onto the European Platform, followed by a rapid middle to late Miocene shortening phase with out-of-sequence thrusting during collision. In the Ukrainian Carpathians, the slow convergence phase took place from the middle Oligocene to the early Miocene (~32 Ma to ~20 Ma). The subsequent rapid contraction phase occurred from the early to the middle Miocene, with an estimated shortening rate of ~21 km/Myr(Nakapelyukh et al., 2018). The deformation of the Inner Carpathian nappes provoked contraction in the adjacent basins and propagating thrusts scraped off sediment sheets from the down-going plate, imbricating them into the wedge. It is estimated that the Ukrainian Carpathians became quiescent at ~12 Ma, when rollback of the European slab and foreland propagation of thrusting ended in the region (Nemčok et al., 2006).

Present-day surface heat flow in the Ukrainian Carpathians, the Pannonian back-arc basin and the European foreland is well constrained. Heat flow in the Pannonian Basin is about 90-100 mW/m², with the highest values recorded close to the Carpathian volcanic arc (Pospisil et al., 2006). Heat flow diminishes across the fold-and-thrust belt, from ~80 mW/m² at the contact with the innermost nappes to values between 40 and 70 mW/m² within the outer nappes (Pospisil et al., 2006). It is possible that Middle Miocene calc-alkaline volcanic intrusions adjacent to the inner nappes, emplaced between 13.8 and 9.1 Ma (Seghedi et al., 2001), provided a transient source of heat, although given the small dimension of the region affected (Horvath et al., 1986), this post-collisional volcanism is unlikely to have had a major impact on heat flow at a regional scale, in line with inferences for the Transylvanian back-arc basin in Romania just to the south of our study area (Tiliță et al., 2018). Another source of transient heat during emplacement of the Carpathian nappes may have been back-arc extension and asthenosphere upwelling under the Pannonian basin between 19 and 15 Ma (Tari et al., 1992; Horváth and Cloetingh, 1996). However, Andreucci et al. (2015) showed that heating associated with Pannonian Basin extension did not affect the Carpathian nappes: low-temperature thermochronology and vitrinite reflectance data indicate a maximum paleo-temperature of 170 °C for the inner part of the wedge, with temperatures decreasing from the middle part of the wedge towards the Pannonian Basin. Well data indicate present-day geothermal gradients in the Skyba nappe ranging from 20 to 24 °C/km (Kotarba and Kołtun, 2006), in broad agreement with the values obtained in external domains of other mountain belts (e.g. Husson and Moretti, 2002). Because tectonic reconstructions of the belt at crustal and lithospheric scale indicate a cylindrical structure (Docin, 1963; Vachtchenko et al., 2003; Gerasimov et al., 2005; Matskiv et al., 2008, 2009), we suggest that an average present-day near-surface geothermal gradient of 25 °C/km may be extrapolated to the entire Carpathian wedge. However, a range of near surface processes can distort the thermal field in orogenic domains. These include in particular the topography that imposes an irregular thermal boundary condition, heat advection in areas undergoing sustained erosion and, conversely, the blanketing effect in domains with rapid sedimentation (e.g., Husson and Moretti, 2002). Because data are scarce, the magnitude of these perturbations and the associated uncertainties can only be inferred indirectly. Nevertheless, expected sedimentation and erosion rates and durations in the region are sufficiently low (< 1 mm/yr, Shlapinskyi 2007; Shlapinskyi et al., 2015; Fig. 2) to only perturb the thermal regime by a maximum of 10 to 15% (Husson and Moretti, 2002). Considering the present-day reference value, this implies that the geothermal gradient could have varied within an approximate range of 22 to 28 °C/km. Thermo-kinematic models could help alleviate this uncertainty, but for the current study, we deem 25 °C/km to be a reasonable estimate.

3 Stratigraphy of the Ukrainian Carpathians

As mentioned above, the Ukrainian Carpathians consist of a number of nappes or thrust sheets, which are differentiated based on their position, stratigraphy and tectonic evolution (Sandulescu, 1988; Ślączka et al., 2005; Oszczypko, 2006). Whereas the stratigraphy of each nappe is to some degree distinct, there are some overarching similarities. Broadly speaking, the Carpathian embayment originated as a passive-margin basin, subdivided by several mostly submarine ridges (known as

cordilleras). Changes in sedimentation patterns in the adjacent parts of the Carpathian embayment indicate that these ridges were periodically uplifted during convergence, possibly by long-distance transfer of compressive stresses (Poprawa and Malata, 2006; Oszczypko et al., 2006). As all the nappes are derived from the Carpathian embayment, their stratigraphic relations retrace the convergence and evolution of the Ukrainian Carpathian wedge before and during accretion. Figure 2 depicts the stratigraphy of the units containing our samples and other units useful for further interpretations. It is mainly based on Ukrainian geological maps (Docin, 1963; Vachtchenko et al., 2003; Gerasimov et al., 2005; Matskiv et al., 2008, 2009) with some exceptions specified below.

In the study region, the Magura nappe (including the Marmarosh domain, following Oszczypko et al., 2005) contains mostly Paleogene sediments, starting with thin-bedded Paleocene flysch followed by an alternation of massive sandstone beds and thin-bedded flysch in the Eocene (Fig. 2). Sedimentation stopped at the Eocene-Oligocene boundary.

The Burkut and Dukla nappes display a very similar stratigraphy from the Lower Cretaceous to the upper Eocene: Early Cretaceous sedimentation started with thin-bedded flysch and limestones as well as some breccia incorporating Jurassic limestones and volcanic rocks. These are followed by sandier deposits in the Upper Cretaceous. In the Paleocene, the sedimentation evolved into a sandy flysch with conglomerate intercalations, followed in the Eocene by thin-bedded flysch varying in thickness throughout the basin. Oligocene sedimentation started with argillites and limestones evolving into thick-bedded sandstones at the top of the Burkut nappe. The youngest sediments of the Dukla nappe consist of grey flysch with thick-bedded sandstones and radiolarites (known as Menilites beds), as well as olistostromes, all deposited in the Oligocene.

Sedimentation in the part of the basin represented by the Krosno nappe started in the Eocene with thick-bedded flysch. The siliceous Menilites beds, which can be followed throughout the Carpathians, mark the base of the Oligocene and are followed by grey argillites and siltstones. The Krosno beds were deposited from the middle Oligocene to the early Miocene, i.e., up to the regional Eggenburgian stage (~18.1 Ma). This particularly thick unit consists of 2 km of sandy flysch sequences with intercalations of olistostromes, argillites, siltstones, and some calcareous layers.

The following nappe in the pile is the Skyba nappe. It is composed of two depositional subunits, an internal unit with an Oligocene stratigraphy resembling that of the Krosno nappe, and an external unit in which Miocene sediments are missing. The oldest sediments in both subunits are dated to the Late Cretaceous and comprise a sequence of thin grey flysch and marl-limestone interbeds with conglomerate lenses. The overlying Paleogene sediments are divided into four suites, alternating between thick-bedded sandstones and thin-rhythmic flysch with conglomerate lenses at the base. These were followed in the Oligocene by the Menilites beds, which evolved into calcareous argillites, grey sandstones with black argillites, and thin sandstones with grey carbonaceous argillites for the internal units. This sequence is topped by Miocene grey argillites with siltstone interbeds deposited until the end of the Eggenburgian (18.1 Ma) in the internal unit. For the external unit, Oligocene deposits, including the Menilites beds, are followed by marls and coarse layered batches of sandstones (Oszczypko, 2006).

Sedimentation in the Boryslav-Pokuttia area began in the Late Cretaceous with argillites intercalated with limestones as well as with some conglomerate lenses. In the Palaeocene, thick sandstones were deposited, followed by an Eocene alternation between thin and thick-bedded flysch deposits. The Oligocene Menilites beds are overlain by sandstones with calcareous siltstones. From the early Miocene to the end of the Eggenburgian, the Boryslav-Pokuttia area accumulated siltstones and clays evolving into thin sandstones, with intercalations of clay. There are also some lenses of conglomerates. A thick layer of argillites and siltstone with lenses of salt was deposited during the Ottnangian (18.1-17.2 Ma, Fig. 2). After this time, sedimentation extended into the Sambir area; while argillites with thin sandstone interbeds accumulated in the Boryslav-Pokuttia area, conglomerates and sandstones were deposited in the area of the current Sambir nappe (Andreyeva-Grigorovich et al., 2008). Sedimentation stopped at the end of the early Miocene in the Boryslav-Pokuttia area, apart from several tens of metres of conglomerates thought to be Pliocene in age. Thick deposits of clay and marls evolving into tuffites and evaporites accumulated, on the other hand, in the Sambir area during the Middle Miocene. Deposition there continued concordantly to the end of the early Sarmatian (10.7 Ma) with grey clays and sandstones with intercalated tuffites. These are

overlain discordantly by syn-tectonic conglomerates dated around 9 Ma (Andreyeva-Grigorovich et al., 2008). In the Ukrainian Carpathians, the middle to late Miocene foredeep is represented by the Bilche-Volytsa Zone, where the oldest sediments are of Badenian age (16-12.65 Ma; Andreyeva-Grigorovich et al., 2008). These show a similar facies as the Badenian deposits of the Sambir nappe, with marls and clays at the base and tuffites intercalated by evaporite layers. Early Sarmatian facies are also similar to those of the Sambir nappe and constitute the uppermost preserved strata in the foredeep. The more distal foreland deposits are shallower-water equivalents of the foredeep sediments.

4 Methods

4.1 Low-Temperature Thermochronology

Low temperature thermochronology can record the thermal evolution of mountain belts and the exhumation of rock in the crust over a large range of temperatures (30 – 300 °C), corresponding to depths of 1-10 km for an average geothermal gradient (e.g., Ault et al., 2019; Malusà and Fitzgerald, 2019). Here we use the apatite fission-track and apatite and zircon (U-Th-Sm)/He low-temperature thermochronometers. These have nominal closure temperatures in the range of 80-120 °C, <80 °C, and <200 °C, respectively, depending on cooling rate, mineral composition and accumulated α-damage (e.g., Ault et al., 2019). When these methods are applied to sedimentary rocks (i.e., in detrital thermochronology), they either record information on the pre-depositional history of the sediments, or on their post-depositional burial and subsequent exhumation, depending on the maximum burial temperature experienced by the samples (e.g., van der Beek et al., 2006; Fillon et al., 2013). In a flysch basin, detrital grains are derived from a variety of source rocks and therefore tend to show a wide range of chemical compositions and apparent cooling ages, if they were not affected by full thermal resetting during burial heating. Thus, detrital thermochronology potentially allows tracing both the pre- and post-depositional history of the sampled sedimentary rocks, if a sufficient number of grains can be analysed per sample (e.g., van der Beek et al., 2006; Fillon et al., 2013; Malusà and Fitzgerald, 2020). The combined thermochronological data can also be used for thermal-history modelling (see section 4.2.1).

4.1.1 Sampling

Fourteen samples, weighing 3-5 kg each, were collected from sandstones across three transects in the Ukrainian Carpathians (Table 1). Sampling focused on areas that were not targeted in previous studies (Andreucci et al., 2015; Nakapelyukh et al., 2018), aiming to collect at least one sample per tectonic unit along each transect (Fig. 1). Samples were crushed and sieved, after which apatite and zircon were separated from other minerals with standard heavy-liquid and magnetic separation techniques. Apatite grains were hand-picked under the microscope for subsequent apatite fission-track (AFT) and apatite (U-Th-Sm)/He (AHe) dating. Zircon (U-Th-Sm)/He (ZHe) dating was performed on the same samples. Most samples yielded sufficient apatite and zircon grains for all three analyses, but in some of the samples, one or two of the analyses were not possible (Table 1).

4.1.2 Fission-track thermochronometry

Eleven samples were prepared for AFT thermochronometry at the Geo-Thermo-Chronology platform of ISTerre, Grenoble (France) using the external detector method (Hurford and Green, 1982). Apatite crystals were mounted in resin, polished and etched with a 5.5M HNO_3 solution at 21 °C during 20 s, and attached to a mica detector. The mounted apatite crystals were irradiated at the Oregon State University Triga reactor (USA). Ten samples contained sufficient countable grains for statistically meaningful dating; AFT ages were only calculated for samples with more than 30 counted grains. Three Durango and three Fish Canyon Tuff standards were used to determine a ζ-calibration value (Hurford and Green, 1983) of

282±12 yr.cm^{-2} for MR. Etch-pit width (Dpar) measurements were made on each analyzed grain in order to determine compositional variations in the apatites, which are known to have an influence on their kinetics (e.g., Carlson et al., 1999; Sobel and Seward, 2010).

4.1.3 (U-Th-Sm)/He thermochronometry

Fracture- and inclusion-free apatite and zircon grains were picked under a microscope; their size was measured and their shape recorded. Of the 11 samples considered, 10 contained apatite and zircon suitable for (U-Th-Sm)/He dating, with one to five single grains of apatite/zircon per sample dated (Tables 3 and 4). ^{4}He concentrations were measure at the University of Potsdam (Germany): crystals were encapsulated and heated by a laser to extract ^{4}He; after mixing with a known amount of purified ^{3}He gas, the gas mixture was analysed in a quadrupole noble-gas mass spectrometer. The crystals were dissolved and their U, Th and Sm content determined by ICP-MS at the German Research Centre for Geosciences (GFZ) Potsdam (Germany) following the methodology of Galetto et al. (2021) and Zhou et al. (2017). AHe and ZHe ages were corrected for α-ejection using the methods outlined by Ketcham et al. (2011).

4.2 Time-temperature models and tectono-stratigraphic analysis

4.2.1 Thermal history modelling

We modelled the time-temperature (T-t) pathways constrained by one or more samples for each of the nappes using the QTQt (version 5.8.0) code (Gallagher, 2012), which employs a Markov chain Monte Carlo inversion method. Inputs for the modelling consisted in our ZHe, AHe, and AFT dates, Dpar values and depositional ages, as well as a limited number (<20 per sample) of fission-track lengths and angles to the c-axis. We used the diffusion model of Gautheron et al. (2009) for AHe and that of Guenthner et al. (2013) for ZHe, as well as the multi-kinetic annealing model of Ketcham et al. (2007) for AFT. For all models we explore a temperature range of 0-300°C and a time range of 350-0 Ma. We included a maximum of two constraints when exploring the T-t space: (1) samples should reside at surface temperatures (5±5 °C) at the depositional age of their host sediment; (2) we imposed a 150±50 °C temperature constraint at 150±50 Ma for the samples belonging to the Magura, Burkut and Dukla units. The latter was applied to force a (partial) reset of the ZHe system in these units before calculation of the burial temperatures after deposition, i.e., the scenario that best complies with our thermochronological results (see below). Inversions were run with 100.000 models for the burn-in and 150.000 models for the post burn-in phases. Model outcomes include a probability field for the range of thermal histories explored as well as several alternative "best-fit" models: The maximum likelihood model is the one that fits the input data the best out of all the burn-in and post-burn-in models, while the "maximum post" model is the post-burn-in model that best fits the data; both may show unwarranted structure, however (Gallagher, 2012). We therefore prefer the "expected" model, which reflects the average of all the tested models, weighted by posterior probability, and its 95% credibility interval to indicate the most probable thermal history recorded by our samples.

4.2.2 Tectono-stratigraphic analysis

The stratigraphy of the wedge (Fig. 2) contains important information on the pre-, syn- , and post-orogenic evolution of the Ukrainian Carpathians: the age, thickness, lithology, depositional environment and provenance of the corresponding sediments provide insight into the former topography and tectonic activity in the region. To complete the post-depositional thermal history, we therefore compiled sedimentary burial diagrams for each sampled unit, using the stratigraphy published on the 1:200,000-scale geological maps of the Ukrainian Carpathians (Docin, 1963; Vachtchenko et al., 2003; Gerasimov et al., 2005; Matskiv et al., 2008 & 2009), which is compiled in Fig. 2. It is notoriously difficult to date flysch deposits, which

contain much reworked fauna, and deformation complicates stratigraphic measurements in the wedge. Keeping this in mind, the stratigraphic data nevertheless provide a useful complement to the thermochronological results. The burial diagrams in Figs. 6 to 9 indicate to which minimal depth samples were buried by sediment accumulation and when the sedimentation rates in the area of the future nappe changed; they also provide a maximum age for cessation of sedimentation. Combined with the thermal history models, this information allows discriminating sedimentary from tectonic burial, and tracking the full burial-exhumation cycle for each nappe. As we are mainly interested in the timing and amount of maximum burial, we made no attempt to correct the burial curves for compaction effects. Sedimentary thicknesses shown in Fig. 2 are averaged for each tectonic unit, resulting in some uncertainty in the thickness of the sedimentary overburden for our samples that can be substantial and increases with progressive burial.

5 Results

5.1 Apatite Fission-Track ages

AFT data are reported in Table 2 and Fig. 3. All samples are characterized by significant age dispersion and $P(\chi^2)$ values close to zero, indicating that they contain multiple age populations. This may be explained by inheritance of a wide variety of detrital grains in our sandstone samples in combination with partial resetting as a result of relatively low temperatures experienced since deposition. In our dataset, samples CAR19-056, -062, -063 and -068 appear relatively close to full resetting, as nearly all single-grain ages are younger than the depositional age (Fig. 3). The rest of the samples contain a large proportion of grains that are significantly older than, or in the range of, the depositional age.

When dealing with significantly dispersed single-grain ages such as here, central ages (Fig. 3, CA) are not geologically meaningful. We therefore used the RadialPlotter program (Vermeesch, 2009) to determine major grain age components (peaks), applying the mixture modelling algorithm of Galbraith and Green (1990) and determining the minimum age (Galbraith and Laslett, 1993) for each sample. Between one and three age peaks were detected in our AFT age distributions (Fig. 3). The youngest peak (P1) generally overlaps within error with the calculated minimum age component (Fig. 3). Minimum ages for samples from the Magura nappe (CAR19-061, -066) range from 24.0 ± 3.3 to 31.0 ± 3.7 Ma, indicating cooling of this nappe before the Miocene (Fig. 3). Samples CAR19-062, 063 and 068 from the Burkut and Dukla nappes are strongly reset and have very similar minimum ages of 11.0 ± 3.0 Ma, 11.0 ± 1.5 Ma, and 10.0 ±1.5 Ma respectively (Fig. 3). These minimum ages are also similar to the 11.0 ± 0.9 Ma minimum age of sample CAR19-069 from the adjacent Krosno nappe, which is partially reset. The minimum age of sample CAR19-070, which derives from a more external position on the Krosno nappe, is 13.0 ± 4.4 Ma. Samples CAR19-045 and 056 from the Skyba nappe display minimum ages of 21.0 ± 2.4 and 16.1 ± 1.0 Ma respectively, the latter being strongly partially reset. Sample CAR19-072, which comes from the same nappe, shows a younger but less precise minimum age of 12.0 ± 6.6 Ma.

In summary, the Magura nappe has partially reset populations with Oligocene minimum AFT age, the Burkut and Dukla nappe have strongly partially reset age distributions with late-Miocene minimum ages, whereas the Krosno and Skyba nappes have partially reset age populations, with minimum ages that generally fall into the early to middle Miocene, except for the innermost part of the Krosno nappe, which has a late-Miocene minimum age, more similar to the Brukut and Dukla nappes.

5.2 Apatite (U/Th)/He ages

AHe data are reported in Table 3 and Fig. 4. Whereas some samples (CAR19-056, -068, -069) show overlapping middle-late Miocene single-grain AHe ages, most samples have widely dispersed ages without a clear correlation with effective Uranium content (eU) or grain size (Supplementary Data Table S1). Although this is to be expected in detrital samples where grains

are characterised by differences in size, eU, as well as pre-depositional thermal history (e.g., Fillon et al., 2013), there are a few single-grain ages that need to be treated with caution. We suspect He loss to have caused anomalously young single-grain ages in samples CAR19-047 and CAR19-62 (Table 3), which we do not consider further. Older AHe ages are to be considered taking into account partial resetting of the AHe system, given the potentially large diversity of radiation damage, grain size and pre-depositional history. This can be the case for samples CAR19-061, -062, -066 and -072, which all have grains with either Paleogene or Miocene AHe ages. We find a relatively large spread of AHe single-grain ages in the Magura and Burkut nappe samples (respectively CAR19-061, -066, -062 and -063). In contrast, samples from the Dukla, Krosno and Skyba nappes, with the exception of CAR19-072, show less AHe-age dispersion. If we do not take into account the AHe ages that are older than the minimum AFT ages of the respective samples, and are therefore clearly partially reset, we find two prominent age peaks in our data: one at 13.5 ± 2.0 Ma and one at 8.8 ± 2.0 Ma. These comprise 70% of the data.

5.3 Zircon (U/Th)/He ages

Zircon (U/Th)/He data are reported in Table 4 and Fig. 5. All but three of the single-grain ages are older than the depositional age of the samples and thus non-reset. Single-grain ages show little correlation with eU or grain size (Fig. A1). The three grains with young ZHe ages (two in sample CAR19-045 and one in CAR19-056) also have suspiciously low U and Th contents and anomalous U/Th ratios (Table 4). A grain from sample CAR19-069 has a ZHe age that is only slightly older than the depositional age and similar characteristics, while a grain from sample CAR19-072 also has very low U and Th content, even though its ZHe age is significantly older than the depositional age. We do not include these grains in our further discussion.

Two clear populations of ZHe ages can be discerned in the remaining grains: 60-130 Ma ZHe ages were obtained from samples from the inner nappes (Magura/Marmarosh, Dukla, Burkut, Krosno) and 230-450 Ma ZHe ages from the outer nappes (Skyba, Boryslav-Pokutia). Because the ZHe ages are demonstrably non-reset, these age groups likely relate to different provenance areas for the detrital zircons in these units.

5.4 Thermal-history models and tectono-stratigraphy

We modelled time-temperature histories for eight samples and briefly summarize the results below, going from the internal to the external nappes. The depositional age of sample CAR19-066, from the Magura nappe, is Lutetian-Bartonian (48-38 Ma; Matskiv et al., 2008). After deposition, it underwent 800±400 m of sedimentary burial until the end of the Eocene (34 Ma). Thermal-history modelling indicates that the sample reached its peak temperature of 85-105 °C around 24-18 Ma, i.e., more than 10 Myr after the end of sedimentation in this area (Fig. 6). The sample subsequently cooled at a constant rate until the present day. There are two interpretations of the stratigraphy of the laterally equivalent Marmarosh nappe (cf. Oszczypko et al., 2005; Matskiv et al., 2009), which influences the inferred amount of burial, but not the depositional age of the corresponding sample CAR19-061. After deposition in the Bartonian-Priabonian (41-34 Ma), the sample underwent 800±200 m of pre-Oligocene burial according to the geological map (Matskiv et al., 2009), whereas ~500 m of additional sedimentary burial is inferred based on the Oszczypko et al. (2005) stratigraphy (Fig. 6). Time-temperature modelling of sample CAR19-061 suggests rapid syn- and post-burial heating to a peak temperature of 85-100 °C, which was reached around 31-29 Ma, with continuous cooling at a constant rate starting ~4 Myr after sedimentation ended.

Next in the direction of vergence of the belt is the Burkut nappe, from which samples CAR19-062 and CAR19-063 were modelled (Fig. 7). Sample CAR19-062 has a Cenomanian-Turonian depositional age (102-89 Ma) and shows a long burial phase under a total of 4000-5000 m of sediment (Matskiv et al., 2009); sedimentation in this area ended in the mid-Oligocene (ca. 28 Ma). Thermal-history modelling reveals a correspondingly long heating phase, with the peak temperature between 105 and 125 °C being reached around 40 Ma. The onset of cooling is difficult to pinpoint exactly for this sample,

but the 95% credible intervals of the expected model show a clear cooling step at ~17.5 Ma. Subsequent cooling was intermittent, with a possible acceleration after 10 Ma (Fig. 7). Sample CAR19-063 has a Danian-Ypresian (65.8-47.8 Ma) depositional age and was buried under 2000-3000 m of sediment until the mid-Oligocene (ca. 28 Ma; Matskiv et al., 2009). Thermal-history modelling indicates that sample CAR19-063 reached a maximum temperature of 110 to 155 °C at 23-18 Ma and began cooling immediately after. Cooling possibly slowed down at around 10 Ma.

Sample CAR19-068 was modelled to retrieve a thermal history for the Dukla nappe (Fig. 8). After deposition in the Campanian-Maastrichtian (83.6-66 Ma), ~3000 m of sediments accumulated on top of the sampled sandstone until the mid-Oligocene (ca. 28 Ma; Matskiv et al., 2008). Thermal-history modelling indicates that heating lasted some 8 Myr longer; the sample reached a peak temperature of 100 to 130 °C at 13 ± 2 Ma, followed by rapid cooling at a constant rate.

Sample CAR19-069 is from the Krosno nappe and was deposited in the Chattian (28-23 Ma). It was subsequently rapidly buried under an overburden of 2500±500 m. Sedimentation in this area terminated in the Early Miocene (Eggenburgian; ~18 Ma; Matskiv et al., 2009). Thermal-history modelling indicates that the peak temperature of 115°C was reached shortly after (~17 Ma), followed by continuous and rapid cooling.

The outermost nappe for which we derived thermal-history models is Skyba. Sample CAR19-045 was deposited in the Lutetian-Bartonian (48-38 Ma; Vachtchenko et al., 2003) and accumulated an overburden of 1700±400 m of sediments until the Burdigalian, when sedimentation stopped. Thermal-history modelling retrieves a most likely onset of burial heating at ~45 Ma and a maximum temperature of 85-100 °C that was reached at 12 ± 1 Ma (Fig. 9). Subsequent cooling was rapid and continuous until the present. Sample CAR19-056 was deposited in the Turonian-Danian (94-62 Ma; Docin, 1963) and accumulated 4000-5000 m of sediment until the Early Miocene (Eggenburgian, ~18 Ma). Thermal-history modelling reveals both syn- and post-depositional heating from ~68 Ma to ~16 Ma, up to a maximum temperature of ~120 °C, followed by rapid and continuous cooling to the present.

6 Interpretation and Discussion

6.1 Burial and exhumation pathways in the Ukrainian Carpathians

The burial diagrams and time-temperature models for the various nappes of the Ukrainian Carpathians obtained in our study provide enhanced insight into the evolution of the orogenic wedge. For several of our samples (CAR19-045, 061, 066, 063, and 069), the peak temperature encountered during burial is very high when compared to the temperatures that would result from sedimentary overburden alone. Moreover, some samples show continued heating after sedimentation had terminated, requiring another process to explain this additional heating.

We identify two ways in which this additional heating may be explained: first, part of the sediment column of the nappes may have been eroded during the evolution of the wedge, which would imply that our burial diagrams are truncated and heating due to sedimentary burial was more intense and continued for longer than we can determine. However, the nappes are internally deformed, so it is unlikely that none of the corresponding sediments would have been preserved in the cores of synclines or under intra-nappe thrusts. The only sediments likely to have been completely eroded are wedge-top deposits that may have accumulated unconformably on top of each of the nappes. There is some evidence that these existed, in the form of the unconformable Radych conglomerate in the Ukrainian Carpathians (Andreyeva-Grigorovich et al., 2008), or the 850-m thick Comanești piggy-back basin in Romania (Dumitrescu et al., 2000). However, accommodation space on the wedge top was probably too limited to explain the observed magnitude of additional heating (corresponding to additional burial of up to 2 km; Fig. 11).

A second and more likely explanation for the additional heating is tectonic burial. In this scenario, sedimentation rate first accelerated as the thrust front prograded over the basin (as shown by several of the burial diagrams; Figs. 6-9), and then

stopped when the site was overthrust by the advancing wedge. The absence of shallow-water facies at the top of the sedimentary column of all but the outermost two nappes (which contain sediments that were deposited on thicker crust), suggests that most of the nappes were overthrust in a deep-water environment. We infer from this observation that sedimentation did not end due to a lack of accommodation space. While we cannot exclude that part of the original sediment column has been eroded, we consider that the observed additional heating is due to tectonic burial. The amount of additional heating, as well as the time lag between the end of sedimentation and the onset of cooling, reflect the relative importance of tectonic thickening due to thrusting and surface erosion in thin-skinned fold-and-thrust belts (Husson and Moretti, 2002; Ehlers and Farley, 2003; Ter Voorde et al., 2004).

To estimate how much tectonic burial a sample underwent, we used a geothermal gradient of 25°C/km for the evolving wedge, as justified in section 2. This allows us to translate the modelled time-temperature paths, based on the thermochronological data, into depths of burial. We note that this approach neglects heat advection and blanketing effects during burial and exhumation. Inferred cooling rates for our samples are all ≤10 °C/Myr, leading to maximum exhumation rates of 400 m/Myr using the estimated geothermal gradient (see above). Maximum burial rates are significantly lower than that, <200 m/Myr for all samples and in the range 50-70 m/Myr for most of them. Such burial and exhumation rates, combined with a detachment depth of 10-15 km (Fig. 1) are not expected to significantly perturb the conductive thermal structure of the fold-and-thrust belt (Husson and Moretti, 2002; Braun et al., 2006). However, the inferred 15% uncertainty in the geothermal gradient (section 2) would lead to a similar relative uncertainty in burial depths. The evolving topography of the wedge could also have affected the thermal structure recorded in particular by the low-temperature thermochronometers AFT and AHe (e.g., Braun et al., 2006). As the topographic evolution of the Ukrainian Carpathians is currently unconstrained, we neglected this effect. The resulting burial and exhumation paths are thus first-order approximations of the evolution of the wedge.

The amount and timing of sedimentary burial, as derived from the nappe stratigraphy, is indicated in the burial diagrams. The amount and timing of tectonic burial can thus be found by subtraction of this amount from the maximum burial inferred from the time-temperature path. The results are shown in Fig. 11. As seen in the regional cross section of Fig. 1, internal thrusting affects each nappe; thus the time-depth model represents only a particular internal thrust slice. Nevertheless, we consider the entire nappe to have behaved more or less according to the thermal models. Finally, assuming that cooling of the sample from the maximum depth of burial to the present-day surface occurred by erosional unroofing, exhumation rates can be calculated for the different nappes of the wedge. This also allows calculation of the total amount of eroded sediment per nappe. Modelled thermal histories can thus be interpreted in terms of sedimentary and/or tectonic burial and subsequent exhumation of the nappe (or unit) they belong to. We use the expected model as the reference for all interpretations of sample pathways.

Interpretation of the modelled thermal histories provides information on the evolution of the Ukrainian Carpathian wedge and highlights the different stages of tectonic burial and final exhumation of the wedge (Fig. 11). The Magura and Marmarosh nappes were accreted at approximately 34 Ma and had a stage of tectonic burial that lasted until 30 Ma in the SE (CAR19-061) and until 20 Ma in the NW (CAR19-066) of our study area. Overthrusting led to 2.5-3 km of tectonic burial in addition to the prior sedimentary burial. Subsequent exhumation amounted to ~4 km, at rates of 0.12-0.14 km/Myr and 0.16-0.22 km/Myr, respectively.

Accretion of the Burkut nappe occurred at ~28 Ma for both samples (CAR19-063 and CAR19-062) and tectonic burial brought them to 5.0 and 5.5 km depth, respectively. The following exhumation stage occurred in two phases: a first phase between 18-10 Ma and a second phase after 10 Ma. The two samples from this nappe have different exhumation rates before 10 Ma (0.22 km/Myr for CAR19-062 and 0.40 km/Myr for CAR19-063); however, this difference may be linked to the lack of time constraints on the peak burial and the initiation of the exhumation stage (especially for CAR19-062), as the timing of the peak temperature impacts directly the exhumation-rate estimate, which is interpolated from this peak to the next

inflexion point of the cooling path. However, the post-10 Ma exhumation rate is ~0.3 km/Myr for both samples and the thickest overburden (up to 5.5 km) was eroded from this nappe. The Dukla nappe shows a long tectonic burial stage, from ~28 Ma to 14 Ma, and started exhuming later than the Krosno and Skyba nappes, which are in a more external position. This timing suggests out-of-sequence thrusting in the Dukla nappe, in line with inferences by Roure et al. (1993). Exhumation of the Dukla nappe started around 12 Ma and occurred at a rate of ~0.38 km/Myr.

The samples of the Krosno nappe (CAR19-069) and the north-west part of the Skyba nappe (CAR19-056) display very similar thermal histories, with a stage of tectonic burial (i.e., accretion) starting at 18 Ma, preceded by rapid syn-orogenic sedimentation on the Krosno nappe (Fig. 2; Shlapinskyi, 2015; Nakapelyukh et al., 2018). Exhumation of these nappes started not long after, at respectively ~17 and ~16 Ma. The southeast part of the Skyba nappe (sample CAR19-045), on the other hand, continued its tectonic burial until 12 Ma. Exhumation rates for the Krosno and Skyba nappes were around 0.3-0.4 km/Myr and 4-5 km of overburden was removed at a significantly higher rate than that of the Burkut and Dukla nappes. We have no thermal-history models for the Boryslav-Pokuttia and Sambir nappes due to their much lower heating, below the level of AFT partial annealing. However, deposition in the Boryslav-Pokuttia area continued until 17.2 Ma (Andreyeva-Grigorovich et al., 2008), while AHe data indicate exhumation at 12.8-9.5 Ma.

We thus observe an apparent increase in exhumation rates from the inner to the outer nappes in our models. However, this could simply be related to the later time of peak burial in the outer nappes, as the lack of track-length measurements lowers the resolution of the thermal history at shallow depths, potentially failing to resolve earlier exhumation to the surface of samples in the inner nappes.

6.2. Evolution of the Ukrainian Carpathian wedge

Our combined tectono-stratigraphic and thermochronological analysis allows us to identify several sedimentary and tectonic events and to retrieve the activity of Ukrainian Carpathian wedge over time. We outline and discuss our main observations of the different stages below.

Several of the burial diagrams show an increase in sedimentation rate just before the corresponding part of the antecedent basin was accreted into the wedge (Fig. 11). Such increasing sedimentation rates are expected in a pro-foreland basin adjacent to an approaching frontal thrust (Naylor and Sinclair, 2008), as has also been suggested for the Polish Carpathians (Poprawa et al., 2002; Oszczypko, 2006). In the Magura area, sedimentation rates increased in the early-middle Eocene, especially in the Marmarosh Unit, until the end of the Eocene (Fig. 2). In the Burkut and Dukla areas, the youngest sediments preserved are middle Oligocene in age; the approach of the active front toward the Burkut and Dukla areas is reflected by a coarsening of the grain size and the occurrence of olistostromes in the flysch, without a marked acceleration of the sedimentation rate. In the Krosno nappe, the two-kilometres-thick Krosno beds show a rapid increase in sedimentation rate within the basin starting in the late Oligocene, probably due to a high sediment supply from the internal Carpathians, uplifted as a result of the growing wedge. Sedimentation in the proximal units of the Skyba area was similar to the Krosno area, with Oligocene sandstones and Miocene syn-orogenic sediments. Miocene layers are absent from the more distal units of the Skyba nappe, where the stratigraphic successions ends with late Oligocene sediments, possibly because of erosion of the overlying strata, or because the external part of the nappe was uplifted while it started to overthrust the Boryslav-Pokuttia area at this time (see Nakapelyukh et al., 2018). The Boryslav-Pokuttia and Sambir nappes preserve the majority of their Miocene deposits, with levels of sandstones and olistostromes followed by evaporite lenses and fossil-rich clays, marking the evolution toward a shallow-marine environment in front of the wedge in the middle Miocene (Fig. 2).

We observe diachronous building of the wedge with periods of increased tectonic activity. For the Magura nappe, the onset of accretion occurred at 34 Ma and exhumation was between 30-22 Ma, coeval with the accretion of the Burkut and Dukla nappes (around 28-22 Ma). Exhumation of the Burkut nappe started immediately afterwards at ca. 20 Ma (Fig. 7) and the next nappes in line, Krosno and Skyba, were being accreted at 18 Ma. Tectonic burial was very rapid for the Krosno nappe

and exhumation started very shortly afterwards (ca. 16 Ma), whereas it occurred later, around 12-8 Ma, for the Skyba nappe (Fig. 8 and 9). Out-of-sequence thrusting in the wedge also occurred during this period, with the onset of exhumation in the Dukla nappe at 14 Ma (Fig. 8). In this scenario, the rapid mid-late Oligocene sedimentation in the Krosno area can be linked to the onset of Carpathian wedge growth and related erosion of the Inner Carpathians.

Exotic pebbles of granite, amphibolite, gneiss, and limestone as well as large blocks of mafic volcanics are only found in the Burkut nappe and in the internal part of the Dukla nappe, in mid-Cretaceous strata, which suggests that a ridge-like basement high was located in the Carpathian embayment in the vicinity of these nappes (Shlapinskyi, 2007; Nakapelyukh et al., 2017; Nakapelyukh et al., 2018). It has been suggested that the arrival of the basement high at the subduction zone may have disrupted the progradation of the wedge and led to the formation of duplexes and out-of-sequence thrusting in the Dukla nappe (Roure et al., 1993). This may also have led to the markedly increased sediment flux to the Krosno area from the Oligocene onward. The basement high might correspond to a south-eastward extension of the Polish Silesian ridge, or a branch of it known as the Bukowiec ridge in the vicinity of the Ukrainian border (Oszczypko, 2006).

Apart from some minor Pliocene conglomerates, the youngest deposits within the Boryslav-Pokuttia nappe are dated to 17.2 Ma (Fig. 2), with local pockets of sediment, only present in the most external parts of the nappe, dated at 13.5 Ma (Andreyeva-Grigorovich et al., 2008). This absence of younger sediments indicates that most of the nappe was tectonically buried just after 17.2 Ma, while syn-tectonic deposition continued locally, and in particular on the more external parts of the nappe, up to 13.5 Ma. The nappe started exhuming simultaneously with the Skyba nappe, as marked by its late-Miocene AHe ages (12.8 ± 0.2 Ma and 9.5 ± 0.1 Ma). Onset of exhumation probably happened when the wedge was thrust over the Sambir area. Badenian (16-12.65 Ma) sediments were found under the Carpathian wedge up to 70 km inward of the frontal thrust (Oszczypko et al., 2006), implying that the Sambir nappe overthrust the foreland by at least this distance after the Badenian. The thrust that delimits the eastern margin of the Sambir nappe, i.e. the Carpathian frontal thrust, crosscuts the early Sarmatian (12.65-11.5 Ma) Dashava formation and must have therefore been active until 11.5 Ma (Andreyeva-Grigorovich et al., 2008). Thrusting ceased afterwards (Nemčok et al., 2006; Nakapelyukh et al., 2018), coincident with the arrival of the wedge at the margin of the rigid East European Platform. Thick-skinned Mesozoic extensional faults on this margin were extensionally reactivated during the Badenian-early Sarmatian phase of wedge propagation and show up to 2.5 km of post-middle-Badenian offset (Krzywiec, 2001). Rheological variations at the margin of the East European Platform (e.g., elastic thickness varies from 40-80 km; Kaban et al., 2018) and the presence of pre-orogenic faults probably determined the location and magnitude of syn-orogenic extension, which occurred 50-70 km away from the orogenic front (Krzywiec et al., 2001; Tărăpoancă et al., 2003, 2004; Leever et al., 2006). The vertical displacement on the normal faults appears to have been higher in the western part of the Ukrainian foreland, decreasing eastward (Oszczypko et al., 2006). The Badenian-Sarmatian depocenter that developed in the hanging wall of these normal faults (~2 km) was subsequently overthrusted by the Sambir nappe.

6.3 Thermochronometric age pattern and wedge dynamics

In line with previous low-temperature thermochronology data (Andreucci et al., 2015; Nakapelyukh et al., 2018), our results indicate partial resetting of the AFT system and fully reset AHe ages in the central nappes (Fig. 10). We find strong partial resetting of the AFT system and full resetting of the AHe system in the Burkut and Dukla nappes, while Andreucci et al. (2015) provided evidence for (strong) partial resetting of the ZHe system in these nappes. In contrast, the AHe and AFT systems are partially reset, and ZHe is non-reset in the innermost Magura nappe. For the more external Krosno and Skyba nappes, AFT samples are variably reset, with less resetting in the outer parts of these nappes. AHe ages, on the other hand, are fully reset in the Krosno nappe. The external part of the Skyba nappe reveals non-reset AHe ages, while the Boryslav-Pokuttia nappe has some reset AHe ages. This pattern of low-temperature thermochronology ages, showing burial heating to maximum temperatures in the core of the wedge (Fig. 10) and decreasing toward both the internal and external limits, is

consistent with the exhumation pattern observed in other orogenic wedges including the Olympic Mountains (Brandon et al., 1998; Batt et al., 2001; Michel et al., 2019); Taiwan (Fuller et al., 2006; Beyssac et al., 2007) and the Apennines (Thomson et al., 2010; Erlanger et al., 2022). It also corresponds to the pattern reproduced in several modelling studies of orogenic wedges (Barr and Dahlen, 1990; Batt et al., 2001; Willett and Brandon, 2002). The increasing thermochronometer ages toward the innermost Magura nappe may indicate that the latter acted as a relatively stable backstop (e.g., Brandon et al., 1998) or that the Ukraine Carpathians constituted an "immature" wedge, where steady state either has not been reached, or has not been maintained sufficiently long to exhume reset thermochronometers within the inner wedge (e.g., Willet and Brandon, 2002; Konstantinovskaia and Malavieille, 2005).

In a theoretical view of orogenic wedges, the accretion of nappes should decelerate over time, i.e., accretion and frontal-thrust propagation should occur with a longer period of quiescence between events as the wedge grows (Naylor and Sinclair, 2007). This does not correspond to our model results. We infer from our time-depth diagrams (Fig. 11) that the accretion-exhumation phases are shorter in the period between 22-18 Ma when the main nappes (Burkut, Dukla, Krosno and Skyba) were accreted. The geodynamic context of this orogen may explain the observed discrepancy. In the Carpathians, the main driver of convergence is the retreat of the subduction zone linked to slab roll-back (Royden and Karner, 1984; Royden, 1993; Wortel and Spakman, 2000; Koněcný et al., 2002). Within this context, orogeny is governed by the dynamics of the slab and, therefore, we infer that dynamic equilibrium of the orogenic wedge could have been impeded by the competition between the accretion of material and the retreat of the orogenic front due to slab roll-back, allowing no time for topography building, thermal re-equilibration or internal deformation. In conclusion, the Ukrainian Carpathians record the competition of orogenic wedge growth and subduction retreat by slab roll-back.

6.4 Sediment provenance from ZHe ages

While the reset and partially reset AFT and AHe thermochronometers provide insight into the sedimentary and tectonic evolution of the wedge, the non-reset ZHe ages provide insights into the sediment supply to the evolving wedge and its precursor deep-water basin (Fig. 12). ZHe ages of this study can be divided in two groups containing ages of 60-130 Ma and 230-450 Ma, respectively. The younger age group is mainly found in the inner nappes (samples CAR19-061, -062, -063; Fig.s 4, 12), while the older ZHe age population (230-450 Ma) is dominant in the outer nappes of the Ukrainian Carpathians (samples CAR19-045, CAR19-047 and CAR19-056; Figs. 4, 12). Whereas ZHe ages reported by Andreucci et al. (2015) are (partially) reset in the core of the orogenic wedge (i.e., in the Burkut and Dukla nappes), their non-reset ZHe ages from the inner (232-250 Ma) and outer (55 and 413 Ma) parts of the wedge provide useful complementary information about sediment provenance.

We interpret the source of the sediment in the inner nappes, characterised by 60-130 Ma non-reset ZHe ages, to be the Bucovinian units of the Inner Carpathians (i.e., basement units of the Dacia plate; Sandulescu, 1988; Schmid et al., 2008) and their sedimentary cover. ZFT studies in the infra-Bucovinian units, located in the Maramures mountains, show fully reset ages recording a cooling phase that started in Cenomanian times (~100 Ma), with another cooling event in the Coniacian-Campanian (90-72 Ma; Gröger, 2006). Sedimentation in the Bucovinian units stopped in Barremian times (129-125 Ma; Krautner, 1975) and the onset of thrusting is dated as Aptian-Albian (125-101 Ma) by the discordant deposition of the Wildflysch formation on top of both units (Sandulescu, 1975). For the Bucovinian and sub-Bucovinian units, which structurally overlie the infra-Bucovinian unit, the ZFT system is generally partially reset, depending on the tectonic overburden and stratigraphic position (Gröger et al., 2008). ZFT ages from the Bucovinian units are very similar to our 60-130 Ma ZHe ages for the innermost nappes, suggesting a source-sink relation. The 232-250 Ma ZHe ages present in the dataset of Andreucci et al. (2015) in the internal nappes may, on the other hand, signify that some zircons were derived from Triassic intrusions that are present in the basement of the inner Carpathian units. In line with our results, provenance analysis

in the Western Carpathians showed that the Magura nappe received sediments from the inner units (Winkler and Slaczka, 1992).

It is well documented that the Silesian, Bukowiec and Dukla basement highs also supplied sediment to the basin, particularly during the Late Cretaceous and early Palaeogene, as demonstrated by crystalline clasts and palaeocurrents in the Burkut, Dukla and Silesian nappes (Oszczypko, 2006). We nevertheless consider it more likely for the zircons with60-130 Ma ZHe ages to have come from the inner Carpathian basement: Supplying zircons with reset ZHe ages from the Dukla ridge would require approximately 6 km of exhumation, which seems unlikely considering that uplift of these ridges occurred due to far-field transmission of compressive stresses related to collision in the Inner Carpathians.

Late Cretaceous to early Palaeocene ZHe ages (60-130 Ma) are dominant in the Eocene to Oligocene of the Krosno nappe, which points towards an Inner Carpathians sediment source, while the basement high had been overthrust by the wedge by this time. In contrast, pre-Oligocene sediments of the Skyba and Boryslav-Pokuttia nappes exclusively display 230-450 Ma ZHe ages, and we infer that sediments in the outer nappes of the Ukrainian Carpathians were initially sourced from an area without significant exhumation (<6 km) since the mid Triassic. Within the context of the Carpathians, the East European Craton and the Teisseyre-Tonrquist Zone are the most plausible sources for these sediments (Pharaoh, 1999; Oszczypko, 2006; Roban et al., 2020). In the Oligocene sediments of the Skyba nappe, zircons from this older ZHe age population are joined by zircons from the 60-130 Ma ZHe age group, suggesting that, in addition to sediment supply from the East European Platform, the area started to receive sediments from the inner Carpathians, either directly or recycled from the evolving wedge.

Our results are in line with recent provenance analyses of sandstones in the Romanian Carpathians based on detrital-zircon U-Pb ages, sedimentology and petrography (Roban et al., 2020, 2022). These indicate that the Cretaceous sediments of the innermost Ceahlau-Severin and Teleajen nappes were sourced from the Bucovinian Units of Dacia basement, while those from the more external Audia, Tarcau and Vrancea nappes were sourced from the European foreland (Roban et al., 2020). The Oligocene series of the Tarcau and Vrancea nappes display coarser-grained lithic-fragment-rich sands and conglomerates that were sourced from both the growing orogenic wedge and thick-skinned nappes of the Inner Carpathians, while the finer-grained quartz dominated sandstones of the Kliwa Fm on the more external part of the same nappes were sourced from the East European Platform (Roban et al., 2022). This mixed provenance signal during the Oligocene is analogous to that recorded in the Krosno and Skyba nappes.

6.5 Sediment recycling in the Carpathian Wedge and sediment supply to the pro-foreland basin

Recycling of sediments is a major process in fold-and-thrust belts; quantifying the amount of eroded material and the timing of erosion can help retrieve sediment fluxes over time. Our study provides a view on the sediment fluxes in the Ukrainian Carpathian wedge from the classic model of a previously accreted nappe providing sediments to the next accreted nappe. A large volume of sediments accumulated in the part of the Carpathian embayment corresponding to the future Burkut, Dukla, Krosno and Skyba nappes during the Oligocene. This sediment cannot have been sourced exclusively from the early thin-skinned wedge, as the amount of material exhumed from the inner nappes at that time was insufficient. Our thermal modelling indicates that during the Oligocene, only the Magura part of the wedge was exhuming. Multiplying the amount of exhumation of the growing wedge, with its width reconstructed from balanced cross-sections (Nakapelyukh et al., 2017, 2018), and comparing the thickness of the sediments over the width of the restored basin, we find an imbalance in the volume of material. In the 30-26 Ma interval, the Magura nappe was embedded in the wedge with a width of 20 km and ~ 0.8 km of exhumed sediment. In the same period, the restored basin carried ~ 1.4 km of sediment over 140 km based on restored sections of the region. For the 26-20 Ma period, the restored section allowed ~ 80 km of width and 0.5 km of

exhumation in the wedge. In comparison, the basin received ~ 4 to 1.5 km of sediment over 30 and 80 km of restored width, respectively. Based on these estimates, the wedge may have provided only 8% and 17% of the basin's sediment during the 30 - 26 Ma and 26 - 20 Ma periods, respectively. This imbalance suggests that much of the syn-orogenic sediment arriving in the basin was rather derived from the Inner Carpathians, or the East-European Platform. The growing wedge itself was a sediment source of minor importance at this time. The Boryslav-Pokuttia area accommodated little sediments after 17.2 Ma, except for deposition in some minor and very localised depocenters in its more external part until ca. 13.5 Ma (Fig. 2; Andreyeva-Grigorovich et al., 2008). However, at that time the Burkut, Dukla, Krosno and Skyba nappes had mostly started exhuming. Hence, a large part of the sediments eroding from the wedge was transported to the Sambir area and/or to the modern Carpathian foreland basin (i.e., the Bilche-Volytsa zone; Figs. 2, 13). In fact, the tectono-stratigraphic analysis, in combination with the kinematics of the Ukrainian Carpathians, indicates very little sediment recycling between the nappes. In the early stages of its development, the wedge provided a limited amount of sediment to the foreland area. During its subsequent rapid growth, most of the sediment eroded from it was first deposited in the Sambir area, and following its accretion, in the modern foreland basin. Pre-orogenic normal faults that were flexurally reactivated created significant accommodation space for the recycled sediment directly in front of the advancing wedge during the final stages of wedge emplacement (Oszczypko et al., 2006).

7. Conclusions

This study adds new constraints on the construction of the Ukrainian Carpathian wedge through low-temperature thermochronology and tectono-stratigraphic analysis. AFT and AHe single-grain ages show partial resetting in the most internal and external nappes and a progression to a very strong partial to total reset with young AHe ages (8-6 Ma) and minimum AFT ages (16-8 Ma) in the central part of the wedge (Burkut and Dukla nappes).

ZHe ages are mainly non-reset, except in the central part of the wedge (i.e., Burkut and Dukla nappes), and shed light on the sediment source areas for the different pre-orogenic basins. A predominance of 130-60 Ma ZHe ages indicates that Eocene to Oligocene sediments in the Magura and Krosno nappes were supplied from the Inner Carpathian basement and/or its sedimentary cover. Partial resetting of the ZHe system hampers provenance analysis for the Burkut and Dukla nappes, but sediment composition suggests that part of their late Cretaceous to early Paleogene sediment was supplied by the intra-basinal Dukla ridge. In the more external Skyba and Boryslav-Pokuttia nappes, sediments older than 35 Ma show 230-450 Ma ZHe ages. We interpret these sediments to have been supplied from the East European Platform. From the Oligocene onwards, zircons from the 130-60 Ma age group also appear in the Skyba nappe, suggesting the arrival of sediment sourced from the Inner Carpathians.

We elucidate the evolution of the wedge by combining burial diagrams and thermal-history modelling, which allows to distinguish sedimentary from tectonic burial for each of the nappes involved. The Magura and Marmarosh areas accumulated sediment until the Eocene; their accretion and exhumation lasted from 34 to 30 Ma and from 34 to 20 Ma respectively. The Burkut and Dukla areas record sedimentation until the Oligocene, while in the Krosno and Skyba areas sedimentation continued into the early Miocene. The Burkut and Dukla nappes started their accretion as the inner nappes began their exhumation, around 28-20 Ma (Fig. 13). For the Burkut nappe, exhumation started at 20-18 Ma, corresponding to the onset of tectonic burial of the Krosno and Skyba nappes. However, the Krosno nappe and the northwest part of the Skyba nappe started exhuming shortly after 18 Ma, in contrast to the south-eastern part of the Skyba nappe that was exhumed around 12 Ma. The more internal Dukla nappe was also exhumed at 12 Ma, probably as a result of out-of-sequence thrusting. Early exhumation in the inner wedge from 34 Ma was slow, with a rate of ~0.1 km/Myr. Following accretion at 28-18 Ma, exhumation occurred at an increasing rate for every progressive nappe (0.2-0.4 km/Myr). Final exhumation of the external nappes after 12 Ma was also rapid, with rates around 0.3 km/Myr. According to these rates and area estimates from balanced

cross sections, eroded sediments from the Ukrainian Carpathian wedge have mainly been transported into the Carpathian foreland basin, with little inter-nappe sediment recycling.

Given the context of a retreating subduction zone and slab roll-back, the Ukrainian Carpathians can be seen as the product of construction of an accretionary wedge in the Oligocene to collision in the late Miocene (Fig. 13). The low-temperature thermochronology pattern of reset versus partially reset ages across the wedge may indicate immature wedge dynamics, as resetting of the thermochronological systems toward the internal part of the wedge should have occurred during its accretion (Willet and Brandon, 2002). The inner nappes were accreted against the basement rocks of the active margin, which functioned as the backstop of the wedge. As convergence continued, the wedge grew through the accumulation of additional thrust sheets (the Burkut and Dukla nappes). The frontal thrust subsequently propagated over an intra-basinal high, which probably triggered the formation of out-of-sequence thrusts. The wedge further propagated during the accretion of the Krosno and Skyba nappes in the early Miocene. In the mid- to late Miocene, roll-back and associated slab suction increased subsidence of the foreland (more than the orogenic load) and reactivated pre-orogenic normal faults of the passive margin. It created an up to 2.5 km deep depocenter in front of the advancing wedge that facilitated its northward propagation, ultimately onto the East European Platform. The foreland was deformed by this last shortening episode until thrusting stopped at 11.5 Ma, coincident with slab detachment (Nemčok et al., 2006).

Data availability

All raw data and analyses can be download here:

Author contributions

AdL acquired funding for the project; AdL and MR planned the field campaign and sampled; MR and MB performed AFT analyses; ERS, MR and JG performed the AHe and ZHe measurements; ERS, MB and PvdB analyzed the data; MR modelled the data and wrote the manuscript draft; AdL, PvdB, LH, ERS and MB reviewed and edited the manuscript.

Acknowledgements

This work is supported by the French National Research Agency in the framework of the "Investissements d'avenir" program (ANR-15-IDEX-02) and is part of the IDEX QUANTIFLUX project. We thank Anton Matoshko for his help during the sampling campaign, and Francis Coeur, Francois Senebier and Melanie Balvay of the GTC platform at ISTerre for their help with sample processing, mineral separation and fission-track thermochronology. Constructive reviews by Piotr Krzywiec and an anonymous reviewer helped to significantly improve the manuscript.

References

Andreucci, B., Castelluccio, A., Jankowski, L., Mazzoli, S., Szaniawski, R., Zattin, M.: Burial and exhumation history of the Polish outer Carpathians: discriminating the role of thrusting and post-thrusting extension. Tectonophysics, 608, 866–883, http://dx.doi.org/10.1016/j.tecto.2013.07.030, 2013.

Andreucci, B., Castelluccio, A., Corrado, S., Jankowski, L., Mazzoli, S., Szaniawski, R., and Zattin, M.: Interplay between the thermal evolution of an orogenic wedge and its retro-wedge basin: An example from the Ukrainian Carpathians, Geol. Soc. Am. Bull., 127, 410–427, https://doi.org/10.1130/B31067.1, 2015.

Andreyeva-Grigorovich, A.S., Oszczypko, N., Ślączka, A., Oszczypko-Clowes, M., Savitskaya, N.A., Trofimovicz, N.: New data on the stratigraphy of the folded Miocene zone at the front of the Ukrainian outer Carpathians. Acta Geol. Pol., 58, 325–353, 2008.

Ault, A. K., Gautheron, C., and King, G. E.: Innovations in (U–Th)/He, fission track, and trapped charge thermochronometry with applications to earthquakes, weathering, surface-mantle connections, and the growth and decay of mountains, Tectonics, 38, 3705–3739, https://doi.org/10.1029/2018TC005312, 2019.

Barr, T. D. and Dahlen, F. A.: Constraints on friction and stress in the Taiwan fold-and-thrust belt from heat flow and geochronology, Geology, 18, 111–115, doi:10.1130/0091-7613(1990)018<0111:cofasi>2.3.co;2, 1990.

Batt, G. E., Brandon, M. T., Farley, K. A., and Roden-Tice, M.: Tectonic synthesis of the Olympic Mountains segment of the Cascadia wedge, using two-dimensional thermal and kinematic modeling of thermochronological ages, J. Geophys. Res. 106, 26731–26746, https://doi.org/10.1029/2001jb000288, 2001.

Beyssac, O., Simoes, M., Avouac, J.-P., Farley, K. A., Chen, Y.-G., Chan, Y.-C., and Goffé, B.: Late Cenozoic metamorphic evolution and exhumation of Taiwan, Tectonics, 26, TC6001, https://doi.org/10.1029/2006tc002064, 2007.

Brandon, M. T., Roden-Tice, M. K., and Garver, J. I.: Late Cenozoic exhumation of the Cascadia accretionary wedge in the Olympic Mountains, northwest Washington State, Geol. Soc. Am. Bull., 110, 985–1009, https://doi.org/10.1130/0016-7606(1998)110<0985:lceotc>2.3.co;2, 1998.

Braun, J., van der Beek, P., and Batt, G. E.: Quantitative Thermochronology: Numerical methods for the interpretation of thermochronological data, Cambridge University Press, 271 pp., 2006.

Carlson, W. D., Donelick, R. A., and Ketcham, R. A.: Variability of apatite fission-track annealing kinetics: I. Experimental results, Am. Mineral., 84, 1213–1223, 1999.

Castelluccio, A., Mazzoli, S., Andreucci, B., Jankowski, L., Szaniawski, R., and Zattin, M.: Building and exhumation of the Western Carpathians: New constraints from sequentially restored, balanced cross sections integrated with low-temperature thermochronometry, Tectonics, 35, 2698–2733, https://doi.org/10.1002/2016TC004190, 2016.

Cloetingh, S. A. P. L., Burov, E., Matenco, L., Toussaint, G., Bertotti, G., Andriessen, P. A. M., Wortel, M. J. R., and Spakman, W.: Thermo-mechanical controls on the mode of continental collision in the SE Carpathians (Romania), Earth and Planetary Science Letters, 218, 57–76, https://doi.org/10.1016/S0012-821X(03)00645-9, 2004.

Dahlen, F. A., Suppe, J., and Davis, D.: Mechanics of fold-and-thrust belts and accretionary wedges: Cohesive Coulomb Theory, J. Geophys. Res., 89, 10087–10101, https://doi.org/10.1029/JB089iB12p10087, 1984.

Davis, D., Suppe, J., and Dahlen, F. A.: Mechanics of fold-and-thrust belts and accretionary wedges, J. Geophys. Res., 88, 1153, https://doi.org/10.1029/JB088iB02p01153, 1983.

Docin, G.D.: State geological map of Ukraine (M34-30) scale 1: 200 000, State geological research institute UkrSGRI, 1963

Dumitrescu, I., Mirăujã, O., Săndulescu, M., Stefănescu, M., Bandrabur, T., Harta Geologică, Republica Socialistă România, scara 1:200.000, tiraj 2000, 1962.

Ehlers, T. A. and Farley, K. A.: Apatite (U–Th)/He thermochronometry: methods and applications to problems in tectonic and surface processes, Earth and Planetary Science Letters, 206, 1–14, https://doi.org/10.1016/S0012-821X(02)01069-5, 2003.

Erlanger, E. D., Fellin, M. G., and Willett, S. D.: Exhumation and erosion of the Northern Apennines, Italy: new insights from low-temperature thermochronometers, Solid Earth, 13, 347–365, https://doi.org/10.5194/se-13-347-2022, 2022.

Farley, K. A., Wolf, R. A., and Silver, L. T.: The effects of long alpha-stopping distances on (U-Th)/He ages, Geochim. Cosmochim. Acta, 60, 4223–4229, https://doi.org/10.1016/S0016-7037(96)00193-7, 1996.

Fillon, C., Gautheron, C., and van der Beek, P.: Oligocene–Miocene burial and exhumation of the Southern Pyrenean foreland quantified by low-temperature thermochronology, J. Geol. Soc. London, 170, 67–77, https://doi.org/10.1144/jgs2012-051, 2013.

Flament, N., Gurnis, M., Müller, R.D., Bower, D.J., and Husson, L.: Influence of subduction history on South American topography, Earth Planet. Sci. Lett., 430, 9–18, doi.org/10.1016/j.epsl.2015.08.006, 2015.

Fuller, C. W., Willett, S. D., Fisher, D., and Lu, C. Y.: A thermomechanical wedge model of Taiwan constrained by fission-track thermochronometry, Tectonophysics, 425, 1–24, https://doi.org/10.1016/j.tecto.2006.05.018, 2006.

Gągała, Ł., Vergés, J., Saura, E., Malata, T., Ringenbach, J.-C., Werner, P., and Krzywiec, P.: Architecture and orogenic evolution of the northeastern Outer Carpathians from cross-section balancing and forward modeling, Tectonophysics, 532–535, 223–241, https://doi.org/10.1016/j.tecto.2012.02.014, 2012.

Gallagher, K.: Transdimensional inverse thermal history modeling for quantitative thermochronology, J. Geophys. Res., 117, B02408, https://doi.org/10.1029/2011JB008825, 2012.

Galetto, A. V., Georgieva, V., Garcia, V. H., Zattin, M., Sobel, E. R., Glodny, J., Bordese, S., Arzadun, G., Bechis, F., Caseli, A. T., Becchio, R.: Cretaceous and Eocene rapid cooling phases in the Southern Andes (36°- 37°S): Insights from low-temperature thermochronology, U-Pb geochronology, and inverse thermal modeling from Domuyo area, Argentina., Tectonics, 40, https://doi.org/10.1029/2020TC006415, 2021.

Gautheron, C., Tassan-Got, L., Barbarand, J., and Pagel, M.: Effect of alpha-damage annealing on apatite (U–Th)/He thermochronology, Chem. Geol., 266, 157–170, https://doi.org/10.1016/j.chemgeo.2009.06.001, 2009.

Gerasimov L.S., Makarov B.O., Chayi S.V., Gerasinova I.I.: State geological map of Ukraine (M34-24) scale 1: 200 000, State geological research institute UkrSGRI, 2005.

Guenthner, W. R., Reiners, P. W., Ketcham, R. A., Nasdala, L., and Giester, G.: Helium diffusion in natural zircon: Radiation damage, anisotropy, and the interpretation of zircon (U-Th)/He thermochronology, Am. J. Sci., 313, 145–198, https://doi.org/10.2475/03.2013.01, 2013.

Handy, M. R., Ustaszewski, K. and Kissling, E.: Reconstructing the Alps–Carpathians–Dinarides as a key to understanding switches in subduction polarity, slab gaps and surface motion, Int J Earth Sci, 104(1), 1–26, doi:10.1007/s00531-014-1060-3, 2015.

Horváth, F. and Cloetingh, S.: Stress-induced late-stage subsidence anomalies in the Pannonian basin, Tectonophysics, 266, 287–300, https://doi.org/10.1016/S0040-1951(96)00194-1, 1996.

Hoth, S., Hoffmann-Rothe, A., and Kukowski, N.: Frontal accretion: An internal clock for bivergent wedge deformation and surface uplift, J. Geophys. Res., 112, B06408, https://doi.org/10.1029/2006JB004357, 2007.

Hurford, A.J., and Green, P.F.: A users' guide to fission track dating calibration, Earth Planet. Sci. Lett., 59, 343-354, 1982.

Husson, L. and Moretti, I.: Thermal regime of fold and thrust belts—an application to the Bolivian sub Andean zone, Tectonophysics, 345, 253–280, https://doi.org/10.1016/s0040-1951(01)00216-5, 2002.

Husson, L., Bernet, M., Guillot, S., Huyghe, P., Mugnier, J-L., Replumaz, A., Robert, X., and van der Beek, P., Dynamics ups and downs of the Himalaya, Geology, 42, 839-842, doi:10.1130/G36049.1, 2014.

Ketcham, R. A., Carter, A., Donelick, R. A., Barbarand, J., and Hurford, A. J.: Improved modeling of fission-track annealing in apatite, Am. Mineral., 92, 799–810, https://doi.org/10.2138/am.2007.2281, 2007.

Ketcham, R. A., Gautheron, C., and Tassan-Got, L.: Accounting for long alpha-particle stopping distances in (U–Th–Sm)/He geochronology: Refinement of the baseline case, Geochimica et Cosmochimica Acta, 75, 7779–7791, https://doi.org/10.1016/j.gca.2011.10.011, 2011.

Konečny, V., Kovač, M., and Lexa, J.: Neogene evolution of the Carpatho-Pannonian region: an interplay of subduction and back-arc diapiric uprise in the mantle, 20, 2002.

Konstantinovskaia, E. and Malavieille, J.: Erosion and exhumation in accretionary orogens: Experimental and geological approaches, Geochem. Geophys. Geosyst., 6, https://doi.org/10.1029/2004GC000794, 2005.

Kotarba, M.J., and Koltun, Y.V.: The origin and habitat of hydrocarbons of the Polish and Ukrainian parts of the Carpathian Province, in Golonka, J., and Picha, F.J., eds., The Carpathians and Their Foreland: Geology and Hydrocarbon Resources. AAPG Memoir 84, p. 395–442, 2006.Kováč, M.: Paleogene palaeogeography and basin evolution of the Western Carpathians, Northern Pannonian domain and adjoining areas, 19, 2016.

Kováč, M.: Paleogene palaeogeography and basin evolution of the Western Carpathians, Northern Pannonian domain and adjoining areas, 19, 2016.

Kovács, I.: Seismic anisotropy and deformation patterns in upper mantle xenoliths from the central Carpathian–Pannonian region: Asthenospheric flow as a driving force for Cenozoic extension and extrusion?, 12, 2012.

Kräutner, H. G., Sassi, F. P., Zirpoli, G., & Zulian, T.: The pressure characters of the pre-Alpine metamorphisms in the East Carpathians (Romania). *Neu. Jb. Mineral., Abh*, *125*(3), 278-296, 1975

Krijgsman, W., and Piller, W.E.: Central and eastern Paratethys regional stages, in Gradstein, F.M., et al., eds., The Geologic Time Scale 2012: Amsterdam, Elsevier, p. 935–937, 2012.

Krzywiec, P.: Contrasting tectonic and sedimentary history of the central and eastern parts of the Polish Carpathian foredeep basin – results of seismic data interpretation, in Marine and Petroleum Geology 18 (2001), Elsevier, p.13-38, 2001.

Malusà, M.G., Fitzgerald, P.G.: From Cooling to Exhumation: Setting the Reference Frame for the Interpretation of Thermochronologic Data. In: Malusà, M., Fitzgerald, P. (eds) Fission-Track Thermochronology and its Application to Geology. Springer Textbooks in Earth Sciences, Geography and Environment. Springer, Cham. https://doi.org/10.1007/978-3-319-89421-8_8. 2019

Malusà, M.G., Fitzgerald, P.G.:The geologic interpretation of the detrital thermochronology record within a stratigraphic framework, with examples from the European Alps, Taiwan and the Himalayas. Earth-Sci Rev. 201,103074. 2020

Matenco, L., Krézsek, C., Merten, S., Schmid, S., Cloetingh, S., and Andriessen, P.: Characteristics of collisional orogens with low topographic build-up: an example from the Carpathians, 22, 155–165, https://doi.org/10.1111/j.1365-3121.2010.00931.x, 2010.

Matskiv B.V., Pukach B.D., Kovalof Y.V., Vorobkanich V.M.: State geological map of Ukraine (M34-29, M34-35, L34-5) scale 1: 200 000, State geological research institute UkrSGRI, 2008.

Matskiv B.V., Pukach B.D., Vorobkaniv V.M., Pastukhanoa S.V., Gnilko O.M.: State geological map of Ukraine (M34-36, M35-31, L34-6, L35-1) scale 1: 200 000, State geological research institute UkrSGRI, 2009.

Mazzoli, S., Jankowski, L., Szaniawski, R., and Zattin, M.: Low-T thermochronometric evidence for post-thrusting (<11 Ma) exhumation in the Western Outer Carpathians, Poland, Comptes Rendus Geoscience, 342, 162–169, https://doi.org/10.1016/j.crte.2009.11.001, 2010.

Merten, S., Matenco, L., Foeken, J. P. T., Stuart, F. M., and Andriessen, P. A. M.: From nappe stacking to out-of-sequence postcollisional deformations: Cretaceous to Quaternary exhumation history of the SE Carpathians assessed by low-temperature thermochronology, Tectonics, 29, https://doi.org/10.1029/2009TC002550, 2010.

Nakapelyukh, M., Bubniak, I., Yegorova, T., Murovskaya, A., Gintov, O., Shlapinskyi, V., and Vikhot, Y.: Balanced geological cross-section of the outer Ukrainian Carpathians along the pancake profile, Journal of Geodynamics, 108, 13–25, https://doi.org/10.1016/j.jog.2017.05.005, 2017.

Nakapelyukh, M., Bubniak, I., Bubniak, A., Jonckheere, R., and Ratschbacher, L.: Cenozoic structural evolution, thermal history, and erosion of the Ukrainian Carpathians fold-thrust belt, Tectonophysics, 722, 197–209, https://doi.org/10.1016/j.tecto.2017.11.009, 2018.

Naylor, M. and Sinclair, H. D.: Pro- vs. retro-foreland basins, Basin Res., 20, 285–303, https://doi.org/10.1111/j.1365-2117.2008.00366.x, 2008.

Nemcok, M., Pospisil, L., Lexa, J., and Donelick, R. A.: Tertiary subduction and slab break-off model of the Carpathian–Pannonian region, Tectonophysics, 295, 307–340, https://doi.org/10.1016/S0040-1951(98)00092-4, 1998.

Nemčok, M., Pogácsás, G., and Pospíšil, L.: Activity Timing of the Main Tectonic Systems in the Carpathian–Pannonian Region in Relation to the Rollback Destruction of the Lithosphere, in: The Carpathians and Their Foreland: Geology and Hydrocarbon Researces: AAPG Memoir 84, edited by: Golonka, J. and Picha, F. J., The American Association of Petroleum Geologists, Tulsa, Oklahoma, U.S.A., 743–766, https://doi.org/10.1306/985627M843083, 2006.

Oszczypko, N.: Late Jurassic-Miocene evolution of the Outer Carpathian fold-and-thrust belt and its foredeep basin (Western Carpathians, Poland), 25, 2006.

Oszczypko, N., Oszczypko-Clowes, M., Golonka, J., and Krobicki, M.: Position of the Marmarosh Flysch (Eastern Carpathians) and its relation to the Magura Nappe (Western Carpathians), Acta Geologica Hungarica, 48, 259–282, https://doi.org/10.1556/AGeol.48.2005.3.2, 2005.

Pharaoh, T. C.: Palaeozoic terranes and their lithospheric boundaries within the Trans-European Suture Zone (TESZ): a review, Tectonophysics, 314, 17–41, https://doi.org/10.1016/S0040-1951(99)00235-8, 1999.

Picha, F. J., Stráník, Z., and Krejči, O.,: Geology and hydrocarbon resources of the Outer Western Carpathians and their foreland, Czech Republic, in J. Golonka and F. J. Picha, eds., The Carpathians and their foreland: Geology and hydrocarbon resources: AAPG Memoir 84, p. 49 – 175. 2006.

Popadyuk I., Vul M., Ladyzhensky G., and Shpak P.: Petroleum geology of the Boryslav – Pokuttya zone, the Ukrainian Carpathians, in Golonka J. and Picha F. J., eds., The Carpathians and their foreland: Geology and hydrocarbon resources: AAPG Memoir 84, p. 455 – 466, https://doi.org/10.1306/985732M843075 , 2006.

Poprawa P., Malata T. and Oszczypko N.: Ewolucja tektoniczna basenów sedymentacyjnych polskiej czêœci Karpat zewnêtrznych w œwietle analizy subsydencji. Prz. Geol., 11 (11): 1092–1108 , 2002. (in Polish with abstract in English)

Ratschbacher, L., Frisch, W., Linzer, H.G., Sperner, B., Meschede, M., Decker, K., Nemčok, M., Nemčok, J., Grygar, R., 1993. The Pieniny Klippen Belt in the western Carpathians of northeastern Slovakia: structural evidence for transpression. Tectonophysics 226, 471–483. https://doi.org/10.1016/0040-1951(93)90133-5

Roban, R. D., Ducea, M. N., Mațenco, L., Panaiotu, G. C., Profeta, L., Krézsek, C., Melinte-Dobrinescu, M. C., Anastasiu, N., Dimofte, D., Apotrosoaei, V., and Francovschi, I.: Lower Cretaceous Provenance and Sedimentary Deposition in the Eastern Carpathians: Inferences for the Evolution of the Subducted Oceanic Domain and its European Passive Continental Margin, Tectonics, 39, https://doi.org/10.1029/2019TC005780, 2020.

Roban, R. D., Ducea, M. N., Mihalcea, V. I., Munteanu, I., Barbu, V., Melinte-Dobrinescu, M. C., Olariu, C., and Vlăsceanu, M.: Provenance of Oligocene lithic and quartz arenites of the East Carpathians: Understanding sediment routing systems on compressional basin margins, Basin Research, bre.12711, https://doi.org/10.1111/bre.12711, 2022.

Roure, F., Roca, E., and Sassi, W.: The Neogene evolution of the outer Carpathian flysch units (Poland, Ukraine and Romania): kinematics of a foreland/fold-and-thrust belt system, Sedimentary Geology, 86, 177–201, https://doi.org/10.1016/0037-0738(93)90139-V, 1993.

Royden, L.H.: The tectonic expression of slab pull at continental convergent boundaries, Tectonics, 12, 303–325, https://doi.org/10.1029/92tc02248, 1993.

Royden, L. and Karner, G. D.: Flexure of lithosphere beneath Apennine and Carpathian foredeep basins: Evidence for an insufficient topographic load, Am Assoc. Petrol. Geol. Bull, 68, 704–712, https://doi.org/10.1306/ad461372-16f7-11d7-8645000102c1865d, 1984.

Royden, L. and Faccenna, C.: Subduction orogeny and the late Cenozoic evolution of the Mediterranean arcs, Ann. Rev. Earth Planet. Sci., 46, 1–29, https://doi.org/10.1146/annurev-earth-060115-012419, 2015.

Sandulescu, M.: Essai de synthèse structurale des Carpathes, Bull. Soc. Géol. France, 299-358., 1975.

Sandulescu, M.: Cenozoic Tectonic History of the Carpathians. In: Royden, L.H. and Horváth, F., Eds., The Pannonian Basin: A Study in Basin Evolution, Am. Assoc. Pet. Geol. Memoir, 45, 17-25, 1988.

Seghedi, I., Downes, H., Pécskay, Z., Thirlwall, M. F., Szakács, A., Prychodko, M., and Mattey, D.: Magmagenesis in a subduction-related post-collisional volcanic arc segment: the Ukrainian Carpathians, Lithos, 57, 237–262, https://doi.org/10.1016/S0024-4937(01)00042-1, 2001.

Şengül-Uluocak, E., Pysklywec, R. N., Göğüş, O. H., and Ulugergerli, E. U.: Multidimensional Geodynamic Modeling in the Southeast Carpathians: Upper Mantle Flow-Induced Surface Topography Anomalies, Geochem. Geophys. Geosyst., 2019GC008277, https://doi.org/10.1029/2019GC008277, 2019.

Shlapinskyi, V.: Geological map of the Ukrainian Carpathians, scale 1: 100 000. Transcarpathian, Ivano–Frankivsk, Lviv, Tscernivtsi regions. In: Krupsky, Yu.Z. (Ed.), Zvit ZAO "Koncern Nadra", Kyiv, 228 p. (in Ukrainian), 2007.

Shlapinskyi, V.: The Geological Architecture of the Skyba, Krosno, DuklyaChornogora Nappes of the Ukrainian Carpathians and Prospects of Oil and Gas (unpublished doctoral thesis). Institute of Geology and Geochemistry of Combustible Minerals, Lviv (in Ukrainian), 2015.

Simpson, G. D. H.: Modelling interactions between fold-thrust belt deformation, foreland flexure and surface mass transport, Basin Research, 18, 125–143, https://doi.org/10.1111/j.1365-2117.2006.00287.x, 2006.

Sinclair, H.: Thrust Wedge/Foreland Basin Systems, in: Tectonics of Sedimentary Basins, edited by: Busby, C. and Azor, A., John Wiley & Sons, Ltd, Chichester, UK, 522–537, https://doi.org/10.1002/9781444347166.ch26, 2012.

Sinclair, H. D., and Naylor, M.: Foreland basin subsidence driven by topographic growth versus plate subduction, Geol. Soc. Am. Bull., 124, 368–379, https://doi.org/10.1130/B30383.1, 2012.

Ślączka, A., Krugłov, S., Golonka, J., Oszczypko, N., and Popadyuk, I.: Geology and Hydrocarbon Resources of the Outer Carpathians, Poland, Slovakia, and Ukraine: General Geology, in J. Golonka and F. J. Picha, eds., The Carpathians and their foreland: Geology and hydrocarbon resources: AAPG Memoir 84, p. 221 – 258. 2006

Sobel, E. R. and Seward, D.: Influence of etching conditions on apatite fission-track etch pit diameter, Chemical Geology, 271, 59–69, https://doi.org/10.1016/j.chemgeo.2009.12.012, 2010.

Sperner, B., Ratschbacher, L., and Nemčok, M.: Interplay between subduction retreat and lateral extrusion: Tectonics of the Western Carpathians. Tectonics, v. 21, 1051, doi:10.1029/2001TC901028, 2002.

Stockmal, G. S., Beaumont, C., and Boutilier, R.: Geodynamic models of convergent margin tectonics: Transition from rifted margin to overthrust belt and consequences for foreland-basin development, Am. Assoc. Petrol. Geol. Bull., 70, 181–190, https://doi.org/10.1306/94885656-1704-11d7-8645000102c1865d, 1986.

Tărăpoancă, M., Bertotti, G., Matenco, L., Dinu, C., and Cloetingh, S. A. P. L.: Architecture of the Focșani Depression: A 13 km deep basin in the Carpathians bend zone (Romania), Tectonics, VOL. 22, NO. 6, 1074, doi:10.1029/2002TC001486, 2003.

Tărăpoancă, M., Garcia-Castellanos, D., Bertotti, G., Matenco, L., Cloetingh, S. A. P. L., Dinu, C.: Role of the 3-D distributions of load and lithospheric strength in orogenic arcs: polystage subsidence in the Carpathians foredeep, Earth Planet. Sci. Lett. 221, p. 163-180, 2004.

Ter Voorde, M., de Bruijne, C. H., Cloetingh, S. A. P. L., and Andriessen, P. A. M.: Thermal consequences of thrust faulting: simultaneous versus successive fault activation and exhumation, Earth Planet. Sci. Lett., 223, 395–413, https://doi.org/10.1016/j.epsl.2004.04.026, 2004.

Tiliță, M., Lenkey, L., Matenco, L., Horváth, F., Surányi, G., and Cloetingh, S.: Heat flow modelling in the Transylvanian basin: Implications for the evolution of the intra-Carpathians area, Global and Planetary Change, 171, 148–166, https://doi.org/10.1016/j.gloplacha.2018.07.007, 2018.

Thomson, S. N., Brandon, M. T., Reiners, P. W., Zattin, M., Isaacson, P. J., and Balestrieri, M. L.: Thermochronologic evidence for orogen-parallel variability in wedge kinematics during extending convergent orogenesis of the northern Apennines, Italy, Geol. Soc. Am. Bull., 122, 1160–1179, https://doi.org/10.1130/b26573.1, 2010.

Vacherat, A., Mouthereau, F., Pik, R., Bernet, M., Gautheron, C., Masini, E., Le Pourhiet, L., Tibari, B., and Lahfid, A.: Thermal imprint of rift-related processes in orogens as recorded in the Pyrenees, Earth and Planetary Science Letters, 408, 296–306, https://doi.org/10.1016/j.epsl.2014.10.014, 2014.

van der Beek, P., Robert, X., Mugnier, J.-L., Bernet, M., Huyghe, P., and Labrin, E.: Late Miocene – Recent exhumation of the central Himalaya and recycling in the foreland basin assessed by apatite fission-track thermochronology of Siwalik sediments, Nepal, Basin Res., 18, 413–434, https://doi.org/10.1111/j.1365-2117.2006.00305.x, 2006.

Willett, S. D. and Brandon, M. T.: On steady states in mountain belts, Geology, 30, 175–178, https://doi.org/10.1130/0091-7613(2002)030<0175:ossimb>2.0.co;2, 2002.

Winkler, W. and Slaczka, A.: Sediment dispersal and provenance in the Silesian, Dukla and Magura flysch nappes (Outer Carpathians, Poland), Geol Rundsch, 81, 371–382, https://doi.org/10.1007/BF01828604, 1992.

Wortel, M.J.R., and Spakman, W.: Subduction and slab detachment in the Mediterranean-Carpathian region, Science, 290, 1910–1917, https://doi.org/10.1126/science.290.5498.1910, 2000.

Zayats, H.B.: Deep Structure of the Western Region of Ukraine Based on Seismic Surveys and Directions for Oil and Gas Prospecting. Publishing house «Tsentr Evropy», Lviv in Ukrainian, 2013.

Zhou, R., Schoenbohm, L. M., Sobel, E. R., Davis, D. W., and Glodny J.: New constraints on orogenic models of the southern Central Andean Plateau: Cenozoic basin evolution and bedrock exhumation, Geological Society of America Bulletin, 129, 152-170, 2017.

Sample	latitude °N	longitude °E	elevation m	Lithology	Tetonic unit	Stratigraphic age Ma	Thermochronometers
CAR19-045	47.9417	25.14956	731	coarse sandstone	Skyba	Lutetian-Bartonian (47.8-37.8)	AFT, AHe, ZHe
CAR19-047	48.3108	25.07353	366	greenish sandstone	Boryslav-Pokuttia	Ypresian (56-47.8)	AHe, ZHe
CAR19-056	48.806	23.79279	626	grey sandstone	Skyba	Upper-Cretaceous (96-66)	AFT, AHe, ZHe
CAR19-061	48.29	23.38376	223	fine, light grey sandstone	Marmarosh	Bartonian-Priabonian (41.2-33.9)	AFT, AHe, ZHe
CAR19-062	48.4893	23.27509	293	fine, light grey sandstone	Burkut	Cenomanian-Turonian (100.5-89.9)	AFT, AHe, ZHe
CAR19-063	48.5132	23.31984	455	grey sandstone	Burkut	Danian-Ypresian (65.8-47.8)	AFT, AHe, ZHe
CAR19-066	48.8085	22.44757	248	white sandstone	Magura	Lutetian-Bartonian (47.8-37.8)	AFT, AHe, ZHe
CAR19-068	48.957	22.61442	296	yellowish sandstone	Dukla	Campanian-Maastrichtian (83.6-66)	AFT, AHe, ZHe
CAR19-069	48.9759	22.8041	460	yellowish sandstone	Krosno	Aquitanian (27.8-23.03)	AFT, AHe, ZHe
CAR19-070	49.1321	23.03773	708	yellow sandstone	Krosno	Eocene (56-33.9)	AFT
CAR19-072	49.3612	23.01119	387	grey sandstone	Skyba	Rupelian (33.9-27.8)	AFT, AHe, ZHe

Table 1: Sample locations and characteristics

Sample	grains	ρ_s	N_s	ρ_i	N_i	ρ_d	$P(\chi^2)$	Dispersion	Central age	2 σ	U	TLn	MTL	Std	Dpar	Dpar err
		10^5 cm^{-2}		10^5 cm^{-2}		10^5 cm^{-2}		%	Ma		ppm		µm		µm	
CAR19-045	75	4.23	1371	18.30	5926	10.80	<<1	48	39.4	6.0	25.0	13.0	11.8	2.3	2.0	0.9
CAR19-056	61	5.03	1230	34.50	8450	10.59	<<1	53	20.3	3.6	49.0	10.0	13.1	2.3	1.7	0.7
CAR19-061	81	4.83	1535	15.50	4937	10.49	<<1	39	47.5	6.6	22.0	21.0	10.8	1.7	1.5	0.8
CAR19-062	67	1.90	488	18.70	4796	10.39	<<1	29	15.9	2.4	27.0	-	-	-	1.7	0.9
CAR19-063	67	1.45	350	16.60	3999	10.29	<<1	41	15.0	2.8	24.0	3.0	12.0	4.0	1.4	1.0
CAR19-066	68	6.55	1247	23.80	4528	10.19	<<1	47	41.1	6.6	35.0	10.0	10.2	2.2	1.5	1.0
CAR19-068	81	1.99	607	25.80	7875	10.09	<<1	25	11.1	1.52	38.0	3.0	8.5	1.6	1.5	1.0
CAR19-069	97	2.53	950	24.10	9043	9.98	<<1	62	16.0	2.8	36.0	9.0	10.5	2.8	1.6	0.6
CAR19-070	31	3.53	360	15.70	1605	9.88	<<1	65	28.1	8.2	24.0	1.0	8.5	0.0	1.5	0.6
CAR19-072	61	2.41	532	15.10	3337	9.78	<<1	59	21.7	4.6	23.0	2.0	13.7	1.2	1.5	0.8

Table 2: Apatite fission-track data. ρ_s: spontaneous track density; N_s: number of spontaneous tracks counted in the sample; ρ_i: induced track density; N_i: number of induced tracks counted on the mica-detector; ρ_d: dosimeter track density; $P(\chi^2)$: Chi-square probability that the sample contains a single age population, U: Uranium content; TLn: number of track lengths measured; MTL: Mean track length; Std: standard deviation of track lengths measurement; Dpar: mean Dpar value for the sample; Dp err: mean error on the Dpar measurement.

Sample	grain	U	Th	Sm	eU	He	ESR	Ft	Uncorrected age	2 σ	Ft corrected ages
		ppm	ppm	ppm	ppm	nmol/g	mm		Ma	Ma	Ma
CAR19-045	045-a1	7.6	18.6	16.5	12.0	0.4	69.08	0.78	6.4	0.2	8.2
	045-a2	4.5	36.1	13.1	13.0	0.9	61.57	0.76	12.9	0.5	17.0
	045-a3	10.4	68.2	24.8	26.4	1.1	88.23	0.83	7.6	0.2	9.2
CAR19-047	*047-a1*	*9.4*	*2.1*	*60.8*	*9.9*	*0.0*	76.87	*0.80*	*0.1*	*0.1*	*0.1*
	047-a2	25.3	31.6	17.6	32.7	1.4	88.18	0.83	7.9	0.1	9.5
CAR19-056	056-a1	24.7	78.8	48.6	43.2	1.7	60.46	0.75	7.4	0.2	9.8
	056-a2	44.7	180.3	22.7	87.1	3.4	65.99	0.77	7.1	0.2	9.2
	056-a3	136.8	194.4	60.3	182.5	6.6	59.30	0.75	6.7	0.1	8.9
CAR19-061	061-a1	4.4	28.1	41.0	11.0	0.7	54.91	0.73	10.6	0.8	14.6
	061-a2	6.6	13.6	23.1	9.8	0.6	62.88	0.76	11.3	0.5	14.8
	061-a3	14.6	5.5	9.1	15.9	1.8	60.81	0.75	20.3	0.7	27.0
CAR19-062	062-a1	12.0	44.8	22.1	22.5	4.0	74.63	0.80	32.8	0.6	41.1
	062-a2	11.0	89.0	4.1	31.9	1.4	62.89	0.76	8.2	0.4	10.7
	062-a3	*1.8*	*45.5*	*5.4*	*12.5*	*0.2*	71.08	*0.79*	*2.7*	*0.1*	*3.5*
CAR19-063	063-a1	5.9	18.7	3.8	10.3	0.4	68.43	0.78	7.3	0.3	9.3
CAR19-066	066-a1	44.9	128.4	6.8	75.1	4.2	70.34	0.79	10.2	0.2	13.0
	066-a2	29.2	22.1	21.6	34.4	8.0	67.91	0.78	42.9	0.7	55.0
	066-a3	7.5	41.7	12.3	17.2	0.6	54.01	0.72	6.5	0.5	9.1
CAR19-068	068-a1	16.0	387.7	52.7	107.1	2.9	63.10	0.76	5.0	0.2	6.6
	068-a2	22.4	291.8	39.1	91.0	2.8	67.40	0.78	5.6	0.3	7.2
	068-a3	27.6	345.9	44.9	108.9	3.2	61.67	0.76	5.4	0.1	7.1
CAR19-069	069-a1	34.9	116.2	7.5	62.2	3.2	68.52	0.78	9.5	0.1	12.2
	069-a2	59.7	242.4	26.5	116.7	5.0	80.53	0.72	7.9	0.1	11.0
	069-a3	37.6	82.8	44.5	57.1	3.5	77.18	0.81	11.1	0.2	13.8
CAR19-072	072-a1	7.6	22.9	11.7	13.0	1.0	66.55	0.77	14.2	0.6	18.4
	072-a2	35.0	5.1	21.8	36.2	4.6	72.61	0.79	23.5	0.3	29.6

Table 3: Apatite (U-Th-Sm)/He data. Ages in italics are considered outliers and were not used in the models and for interpretations. eU: equivalent Uranium content; ESR: equivalent spherical radius; 2σ: weighted 2σ analytical uncertainty from analysis of age standards.

Sample	grain	U	Th	Sm	eU	He	ESR	Ft	Uncorrected age	2 σ	Ft corrected ages
		ppm	ppm	ppm	ppm	nmol/g	mm		Ma	Ma	Ma
CAR19-045	*045-z1*	*2.3*	*28.6*	*0.7*	*9.0*	*0.9*	*79.5*	*0.80*	*19.2*	*0.6*	*24.2*
	045-z2	*0.8*	*5.3*	*0.3*	*2.0*	*0.1*	*57.6*	*0.77*	*8.5*	*2.4*	*11.0*
	045-z3	483.7	74.9	0.6	501.4	704.9	83.6	0.85	254.9	2.3	298.5
CAR19-047	047-z1	66.0	62.8	0.4	80.8	164.9	105.4	0.88	367.3	2.6	417.4
	047-z2	54.1	73.8	0.7	71.5	71.4	61.4	0.79	182.6	4.7	229.1
CAR19-056	056-z1	52.3	77.3	0.5	70.5	150.2	55.4	0.77	383.1	15.7	491.7
	056-z2	*2.4*	*70.1*	*2.5*	*18.8*	*1.2*	*70.8*	*0.81*	*11.8*	*0.8*	*14.6*
	056-z3	98.8	123.4	1.0	127.8	259.7	80.9	0.84	365.9	4.8	432.3
	056-z4	41.8	25.5	0.2	47.7	71.8	72.1	0.83	272.8	3.3	328.7
CAR19-061	061-z1	212.4	61.2	0.3	226.8	111.2	60.4	0.80	90.3	0.8	113.2
	061-z2	274.9	132.0	0.6	306.0	121.2	67.0	0.81	73.0	0.9	89.6
	061-z3	345.3	74.8	0.6	362.9	135.8	64.1	0.79	69.0	0.8	87.0
	061-z4	853.2	260.8	1.3	914.4	364.2	61.9	0.80	73.4	0.5	91.6
	061-z5	111.5	43.8	0.6	121.7	63.2	65.6	0.81	95.5	1.2	117.6
CAR19-062	062-z1	47.0	35.7	0.3	55.4	31.6	66.8	0.81	104.6	1.4	128.6
	062-z2	204.8	190.1	2.5	249.5	120.6	61.9	0.79	88.9	1.8	112.4

	062-z3	74.6	111.8	0.4	100.8	58.3	72.2	0.82	106.1	1.3	128.7
	062-z5	167.8	55.6	0.5	180.9	87.9	56.6	0.78	89.4	1.5	114.0
	063-z1	39.9	51.4	0.2	52.0	20.9	76.5	0.83	73.8	0.8	89.0
	063-z2	65.1	39.8	0.1	74.5	40.6	68.3	0.81	100.3	1.0	123.5
CAR19-063	063-z3	144.9	55.9	0.2	158.1	95.2	106.2	0.88	110.7	2.2	125.5
	063-z4	534.8	60.5	0.5	549.0	411.5	55.1	0.78	137.4	1.6	175.9
	063-z5	372.9	197.6	3.1	419.3	165.8	39.1	0.69	72.8	1.2	105.1
	066-z1	211.9	35.0	0.7	220.1	98.5	64.4	0.81	82.4	1.3	101.8
	066-z2	115.1	184.1	1.1	158.4	86.4	83.3	0.84	100.2	1.7	118.9
CAR19-066	066-z3	125.5	140.1	1.5	158.4	190.9	44.8	0.72	219.4	3.7	300.7
	066-z4	272.4	34.4	0.5	280.5	85.3	56.7	0.78	56.2	0.7	71.6
	066-z5	24.6	23.1	0.3	30.0	12.5	67.6	0.81	76.4	1.3	94.6
	068-z1	227.7	135.7	0.6	259.6	307.2	65.5	0.81	215.4	2.4	265.1
CAR19-068	068-z2	737.8	141.3	1.2	771.0	522.2	66.8	0.81	124.3	1.6	152.2
	068-z3	132.6	26.8	0.2	138.9	146.8	72.7	0.83	192.7	1.8	231.6
	069-z1	106.0	12.6	0.1	109.0	99.3	59.3	0.79	166.6	2.2	209.2
	069-z2	124.5	67.4	0.3	140.3	58.5	57.8	0.79	76.9	1.5	97.7
CAR19-069	069-z3	124.3	93.5	0.8	146.3	39.9	60.7	0.79	50.4	0.6	63.4
	069-z4	126.2	87.3	0.3	146.7	68.4	62.3	0.80	85.9	1.4	107.2
	069-z5	*0.7*	*8.6*	*2.9*	*2.7*	*0.5*	66.0	*0.80*	*34.5*	*1.8*	*43.4*
	072-z1	405.6	120.0	0.6	433.8	185.5	58.6	0.79	78.8	0.8	99.6
CAR19-072	*072-z2*	*0.5*	*3.4*	*2.1*	*1.3*	*0.8*	*60.1*	*0.78*	*105.5*	*4.0*	*135.0*
	072-z3	495.9	266.7	3.4	558.5	516.8	62.6	0.80	169.1	2.4	210.3

Table 4: Zircon (U-Th-Sm)/He data. Ages in italics are considered outliers and were not used in the models and for interpretations. eU: equivalent Uranium content; ESR: equivalent spherical radius; 2σ: weighted 2σ analytical uncertainty from analysis of age standards

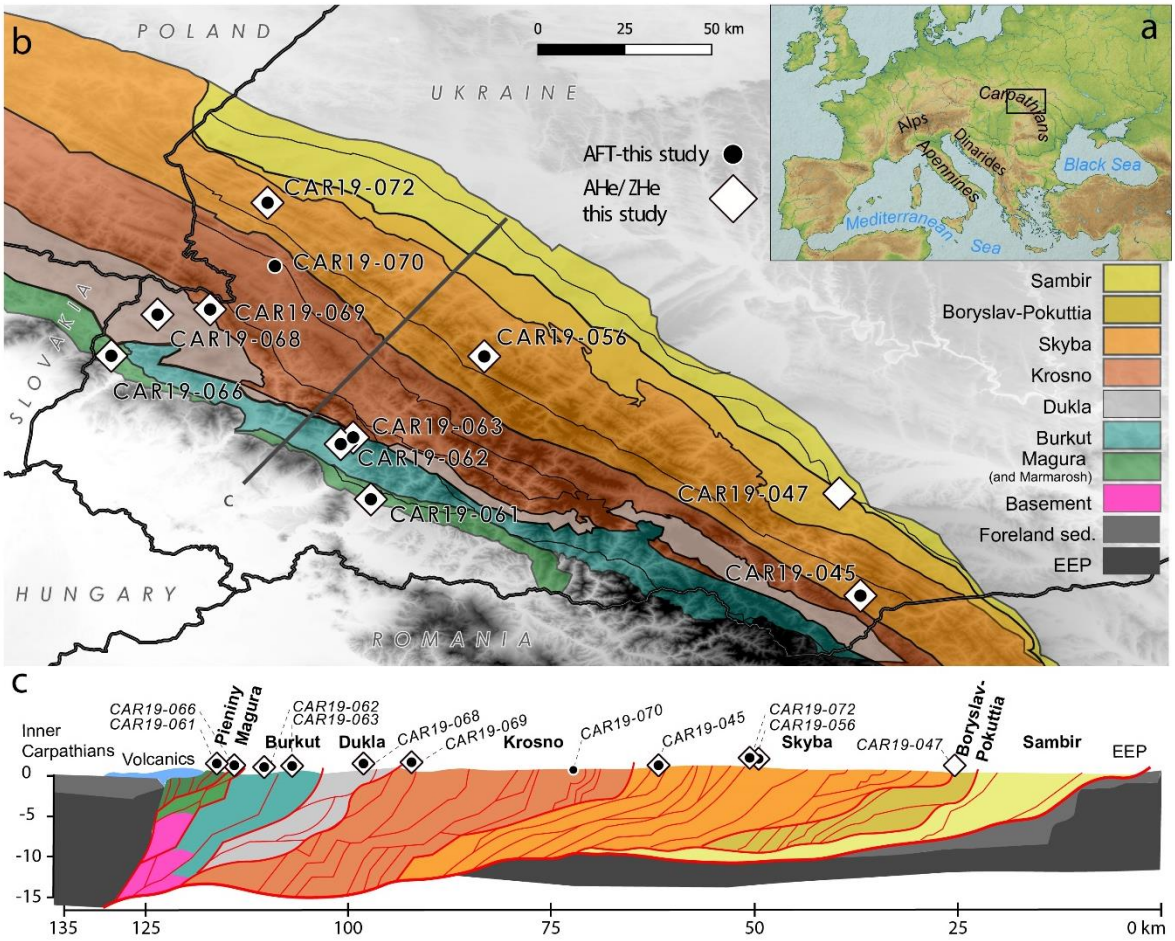

Figure 1: Overview of study area in the Ukrainian Carpathians, showing the main tectonic nappes and sample locations. a) Inset shows setting of the Carpathian belt in Europe and location of the study region. b) Simplified tectonic map; units are highlighted in different colours and follow Schmid et al. (2008), with revised names to more closely follow the regional designation of the lithostratigraphy; EEP: East European Platform. The Marmarosh and Magura nappes are both represented in green. Thin lines represent major intra-nappe faults. Grey thick line marks the location of the cross section. c) Simplified tectonic cross section (after Nakapelyukh et al., 2018). Major faults delimiting the nappes are in bold red lines, thin red lines indicate intra-nappe faults. Sample locations are projected onto the section.

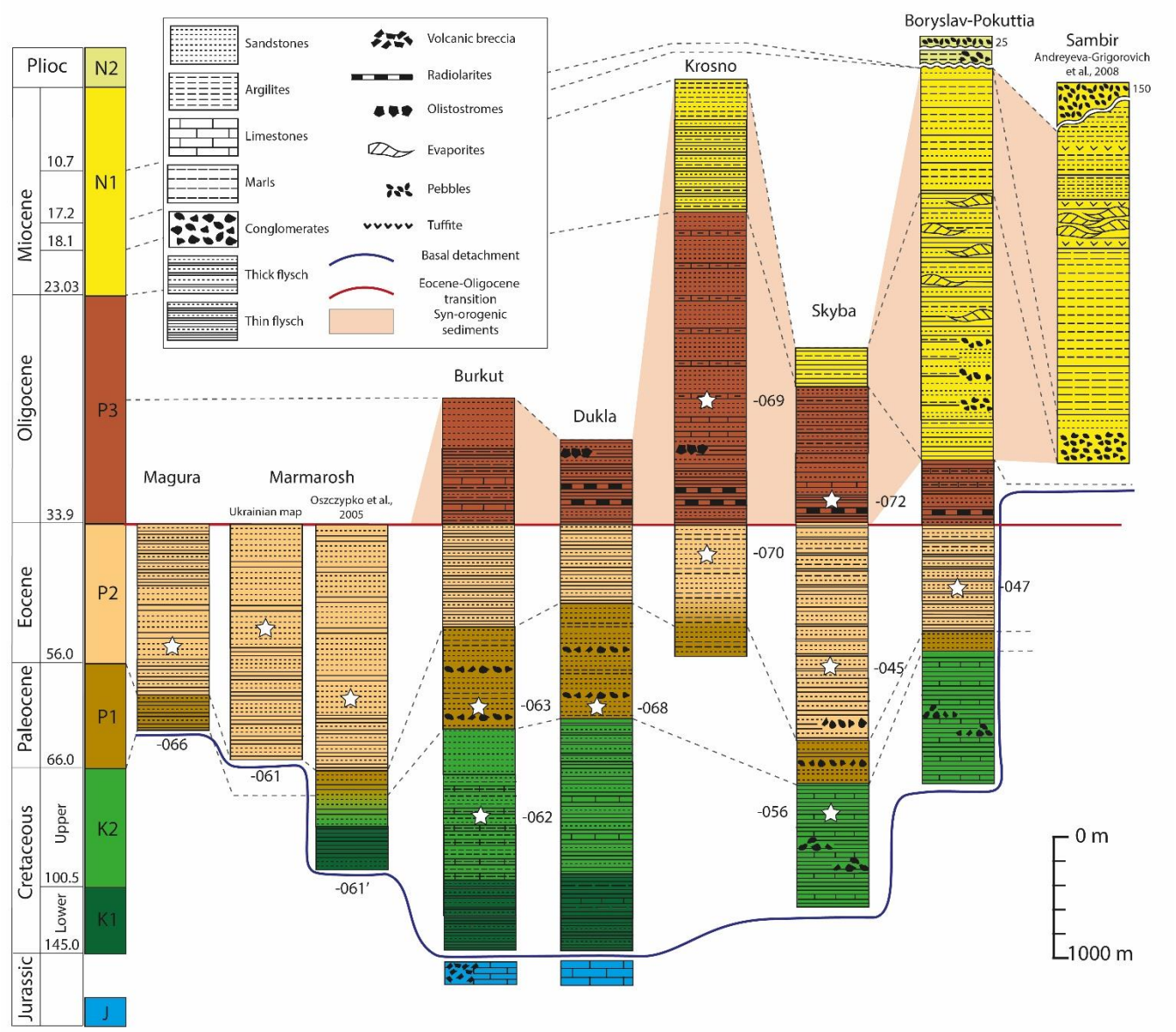

Figure 2: Regional stratigraphy of the Ukrainian Carpathian nappes, mainly from Ukrainian geological maps (Docin, 1963; Vachtchenko et al., 2003; Gerasimov et al., 2005; Matskiv et al., 2008, 2009). Stars mark the sample locations in the nappe stratigraphy; samples are identified by their suffix. Dark blue line marks the décollement horizon of the nappes. Jurassic rocks are integrated in the Burkut and Dukla nappes. Syn-orogenic sediments are indicated in the beige zone, older deposits are regarded as pre-orogenic. Any syn-orogenic sediments on the Magura and Marmarosh nappes have been eroded. Two interpretations of the stratigraphy are indicated for the Marmarosh nappe: one from the Ukrainian geological map; the other from Oszczypko et al. (2005). The Sambir nappe stratigraphy is after Andreyeva-Grigorovich et al. (2008), adapted to the revised stratigraphic limits of Paratethys stages (Krijgsman and Piller, 2012). The stratigraphic columns depicted here are the closest ones available to

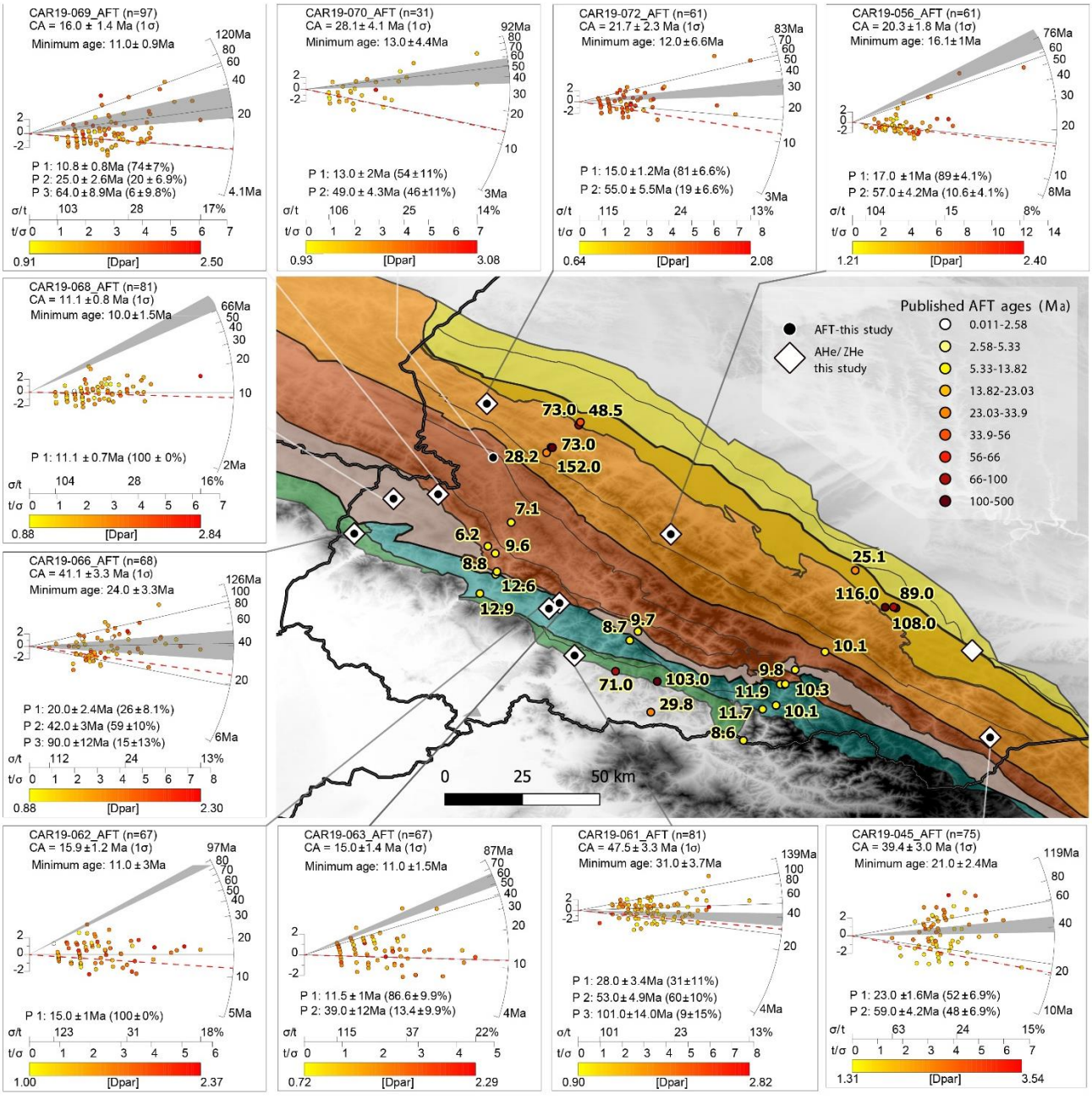

the sampling site of each sample. Lateral variations in thickness or nature of deposition within individual nappes are not represented by these logs.

Figure 3: AFT data from this study shown as radial plots (centred on the central age, which is reported below the sample code as CA); individual single-grain ages in radial plots are coloured according to Dpar value. Grey band in radial plots indicates depositional age, dashed lines are different age populations (P1, P2, etc.); red dashed line is minimum age. Coloured circles on map show AFT central ages from previous studies (Nakapelyukh et al., 2017, 2018; Andreucci et al., 2013, 2015). Base map shows different nappes, with colour scheme as in Figure 1.

Figure 4: Apatite (U-Th)/He ages in the Ukrainian Carpathians. Symbols and colour scale for the data are as indicated in Figure 3. Single-grain ages, corrected for α-ejection, from this study are detailed next to the map frame (numbers in parentheses next to sample code denote the depositional age range). Previously published data (Andreucci et al., 2013, 2015; Merten et al., 2010) are reported on the map as the average age and associated uncertainty, with maximum and minimum single-grain ages below. Ages in grey are interpreted to be outliers and are not used in the models or in our interpretations.

Figure 5: Zircon (U-Th)/He ages in the Ukrainian Carpathians. Symbols and colour scale for the data are as indicated in Figure 3. Single-grain ages, corrected for α-ejection, from this study are detailed next to the map frame (numbers in parentheses next to sample code denote the depositional age range). Previously published data (Andreucci et al., 2015) are reported on the map as follow: -depositional age range, - average age and associated uncertainty, - maximum single-grain age, - minimum single-grain age. Ages in grey are interpreted to be outliers and are not used in the models or in our interpretations.

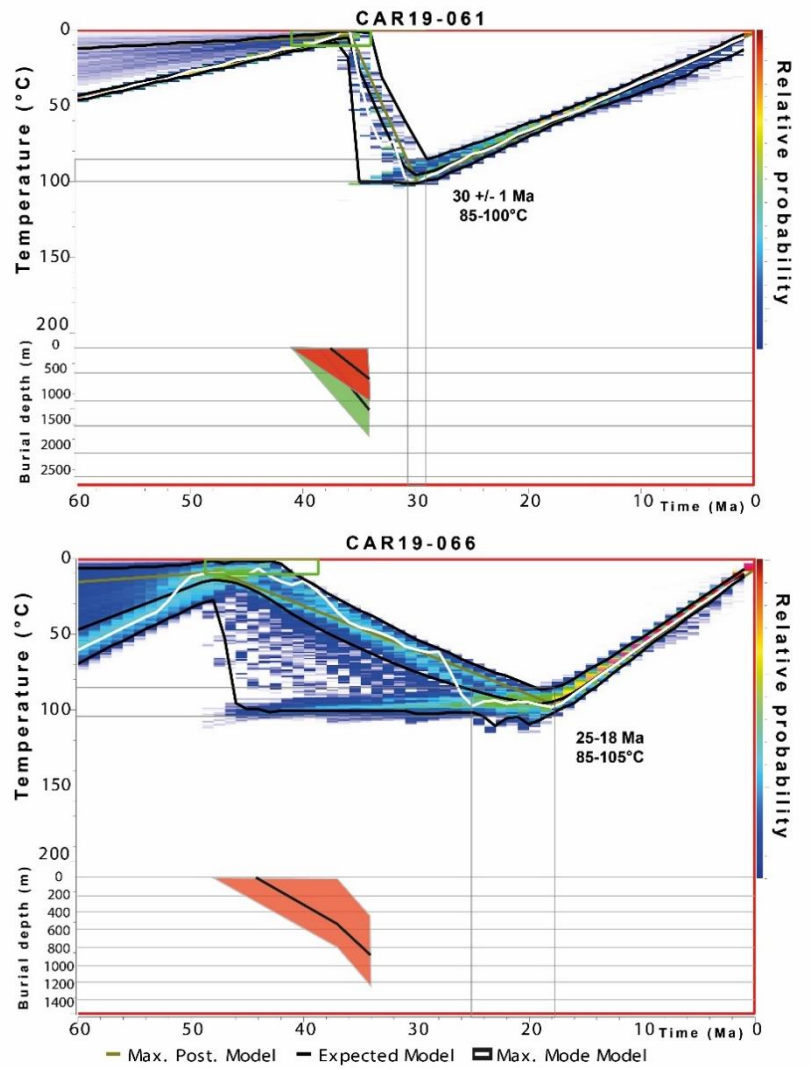

Figure 6: Modelled thermal histories and associated burial diagrams for samples CAR19-061 and -066 from the Marmarosh and Magura nappes, respectively. For sample CAR19-061, burial diagrams are shown both for the stratigraphy from the Ukrainian geological map (orange) and the revised stratigraphy proposed by Oszczypko et al. (2005; green) as shown in Fig. 2. Peak burial temperature and time are highlighted by grey boxes.

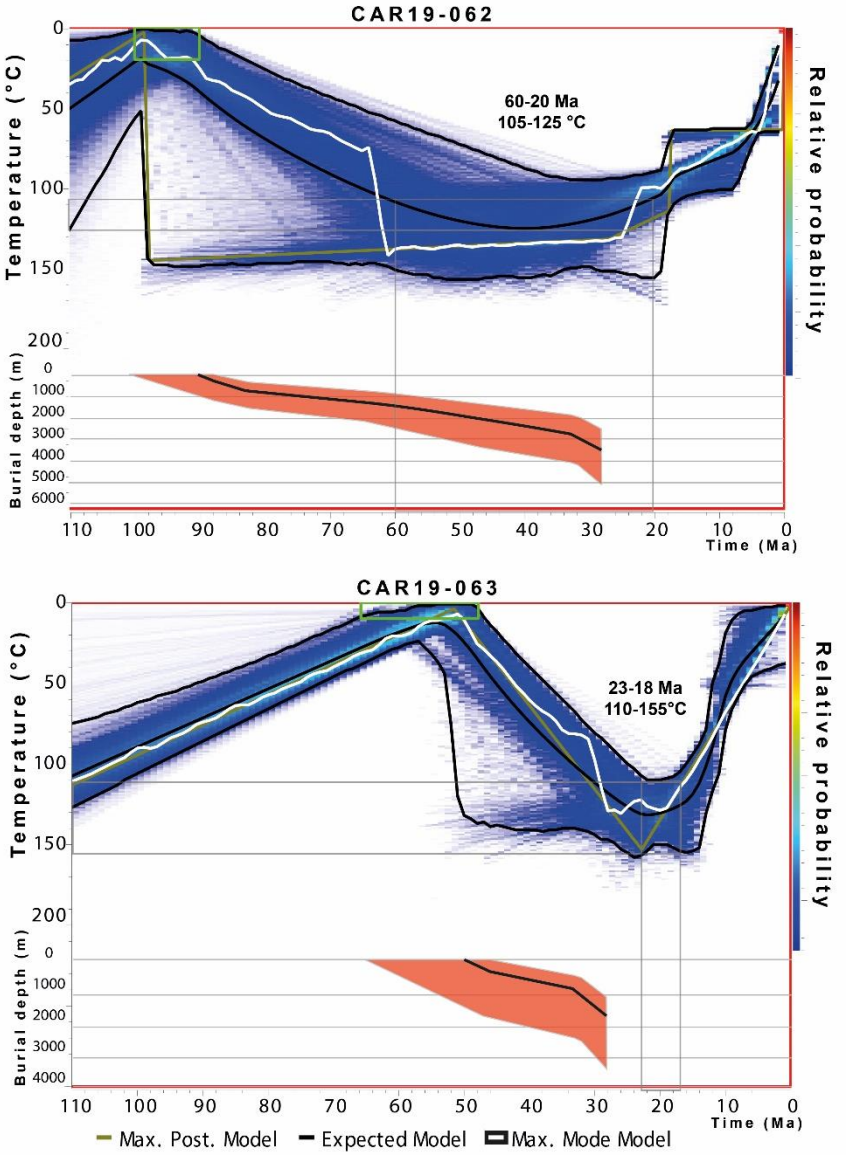

Figure 7: Modelled thermal histories and associated burial diagrams for samples CAR19-062 and 063 from the Burkut nappe. Peak burial temperature and time are highlighted by grey boxes.

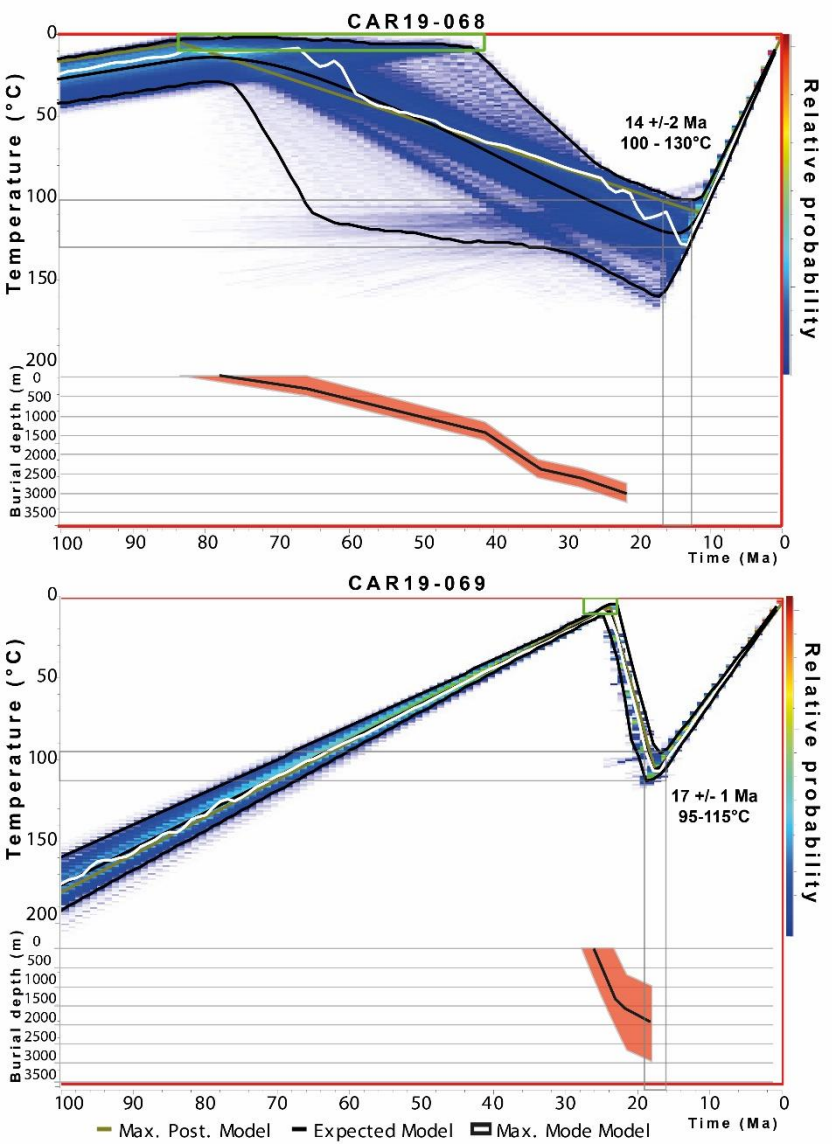

Figure 8: Modelled thermal histories and associated burial diagrams for samples CAR19-068 and 069 from the Dukla and Krosno nappe, respectively, and associated burial diagrams. Peak burial temperature and time are highlighted by grey boxes.

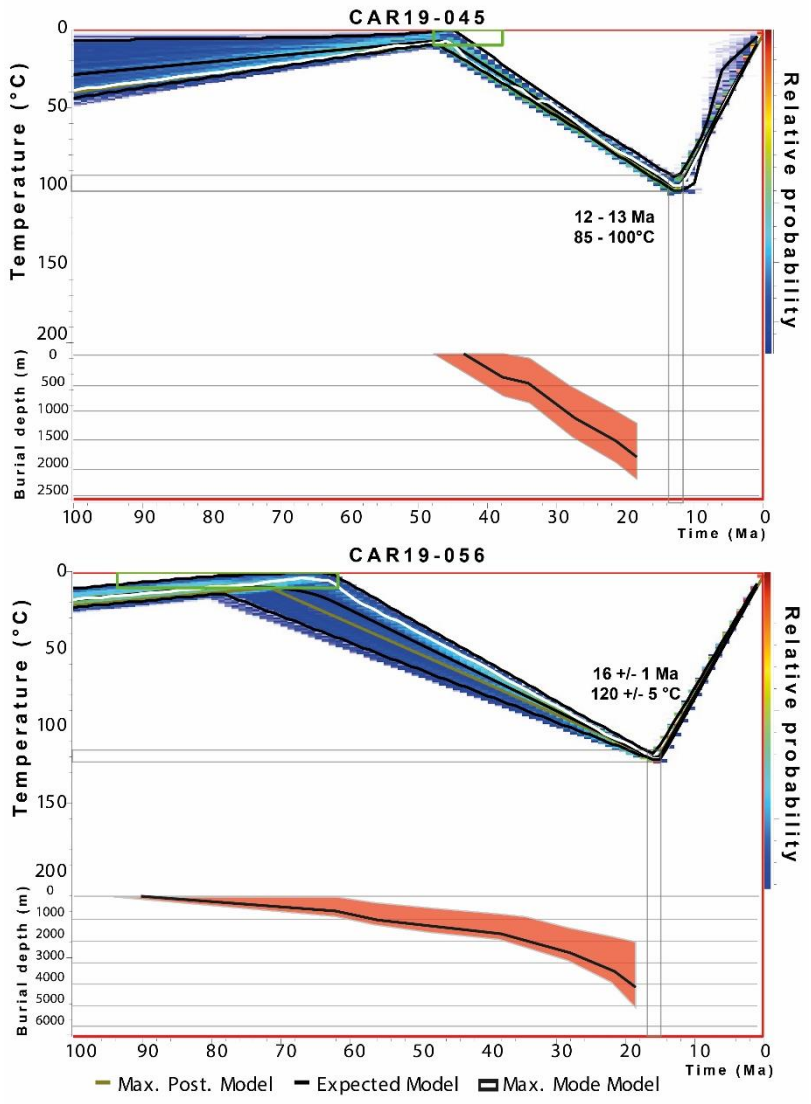

Figure 9: Modelled thermal histories and associated burial diagrams for samples CAR19-045 and -056 from the Skyba nappe and associated burial diagrams. Peak burial temperature and time are highlighted by grey boxes.

Figure 10: Distribution of thermochronometer ages across the Ukrainian Carpathians as a function of distance, measured from the inner belt to the outer belt. The figure shows a compilation of previously published ages with symbols according to the system; samples from this study ages are shown with stars. Single-grain AHe and ZHe ages are shown; AFT data are represented as central ages together with the 2σ error. Note that the age axis is logarithmic. Curves outline the overall age pattern.

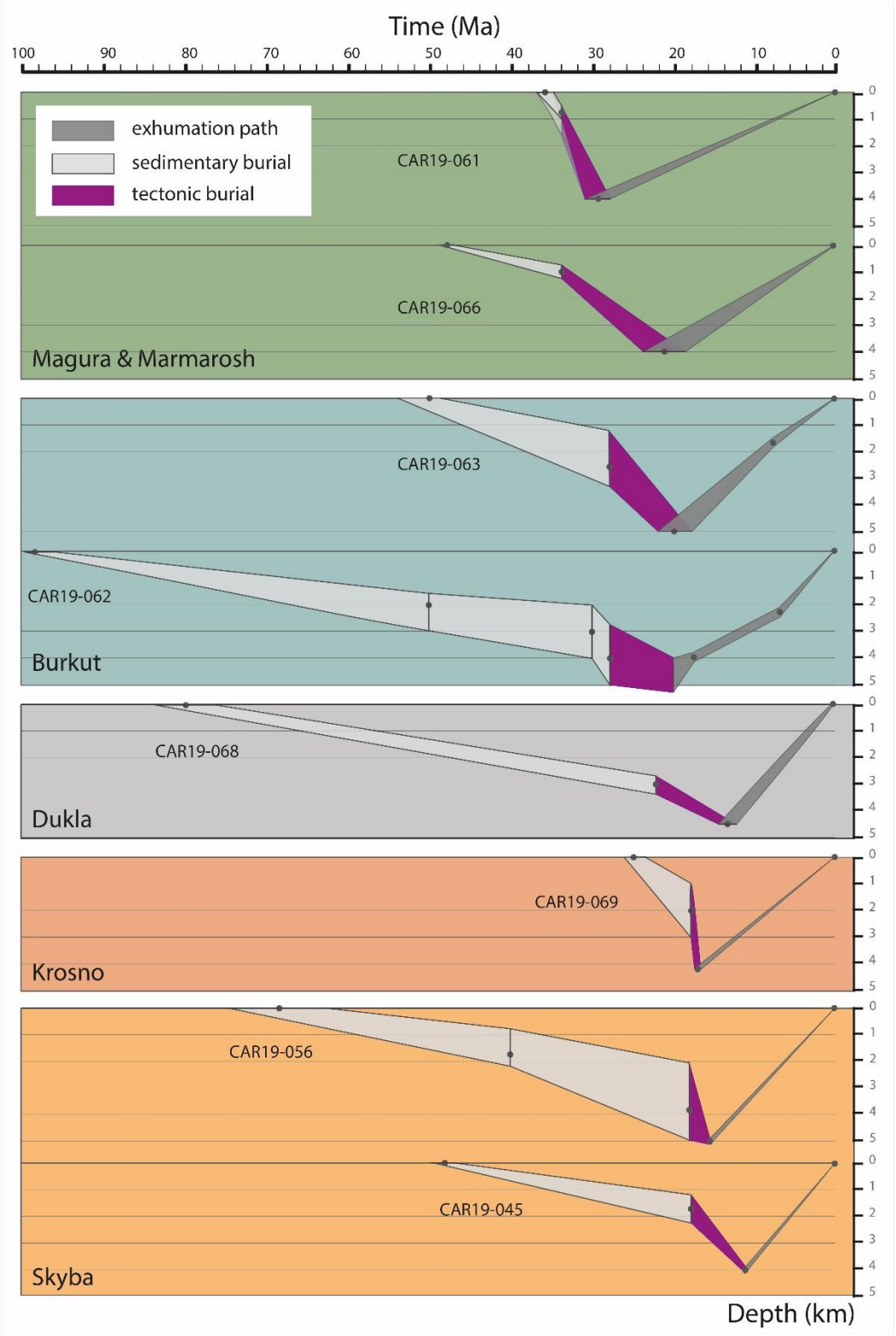

Figure 11: Time-depth evolution of each sample. The depths of the samples through time was estimated from the burial diagrams and the thermal histories modelled in Figs. 7-10, using a geothermal gradient of 25°C/km. Tectonic burial refers to the accretion and burial by thrusting. Time-depth paths are sorted from the innermost (top) to the outermost sample (bottom) of this study. Box colours represent each tectonic nappe as in Figure 1.

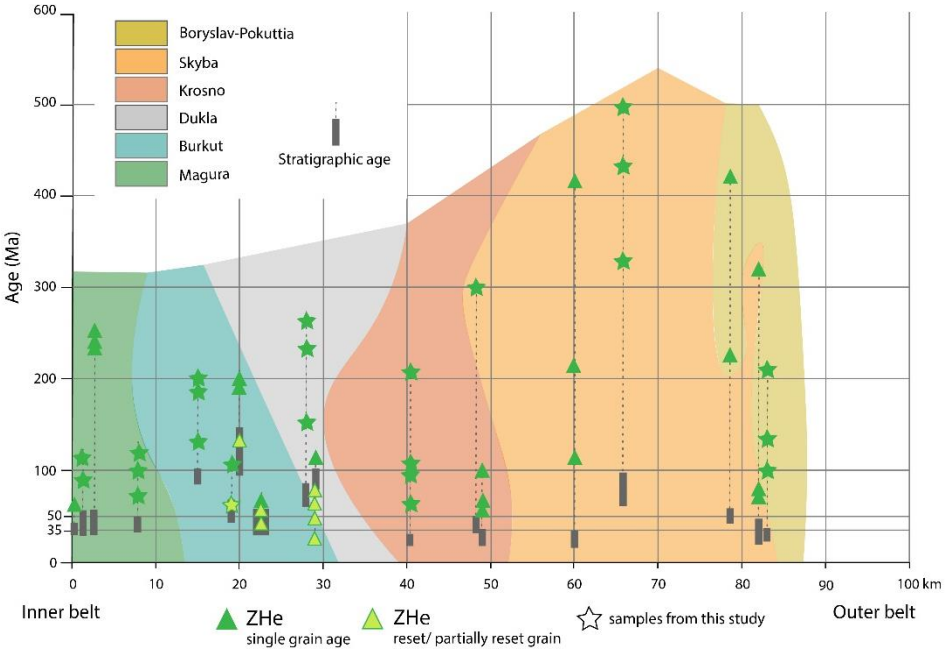

Figure 12: Distribution of ZHe ages across the Ukrainian Carpathians as a function of distance from the inner to the outer belt. Stars represent data from this study; triangles are previously published data. Grey boxes indicate the stratigraphic age of the sample and dashed line mark the corresponding thermochronological ages. Coloured areas represent the different nappes.

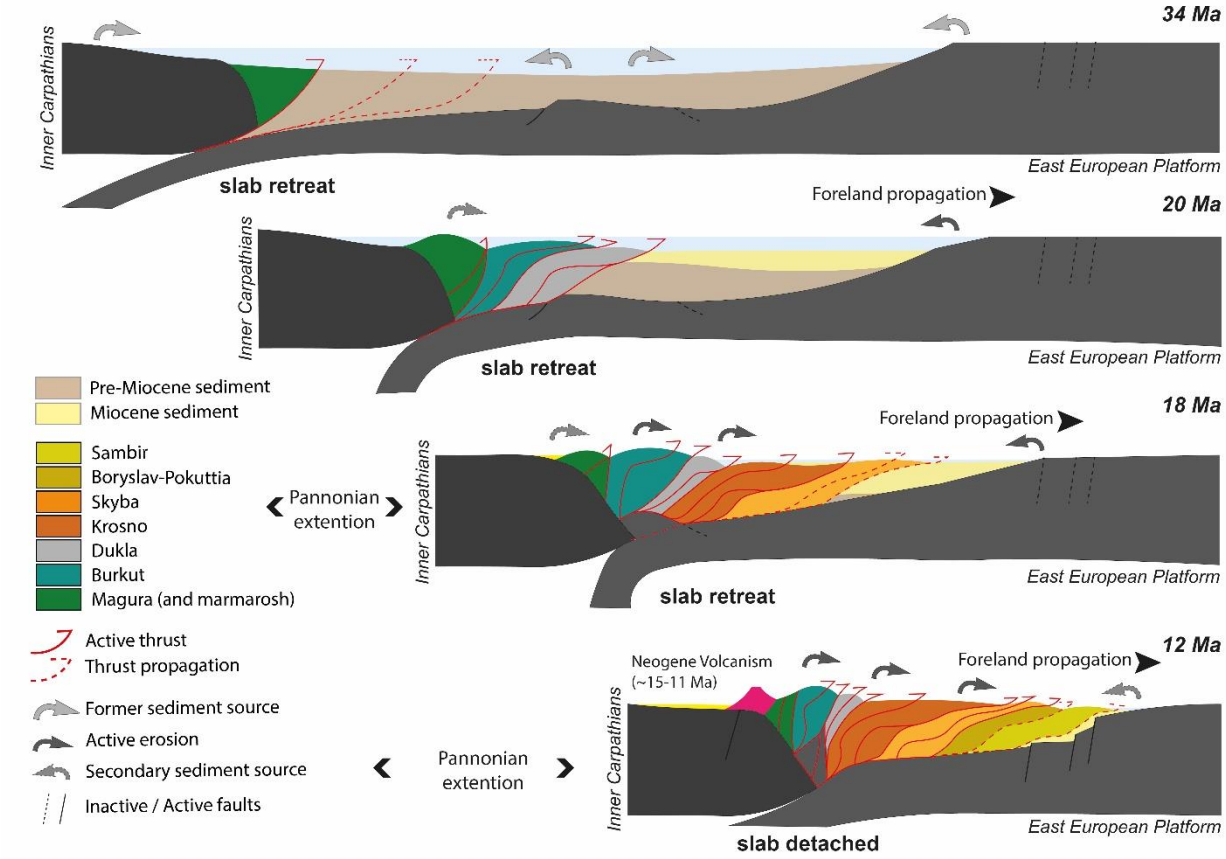

Figure 13: Sketch of the construction of the Ukrainian Carpathian wedge from 34 Ma to 12 Ma. Dashed red line are thrusts that will propagate on the next time step. Full red lines with arrows on top are thrust that are active or will reactivate, full red lines without arrows are sealed. Light grey arrows show source of sediment supply to the different basins. Dark grey arrows are for the active erosion of the nappe. For 12 Ma sketch, foreland propagation terminated around 11.5 Ma (Nemčok et al., 2006). Not to scale.

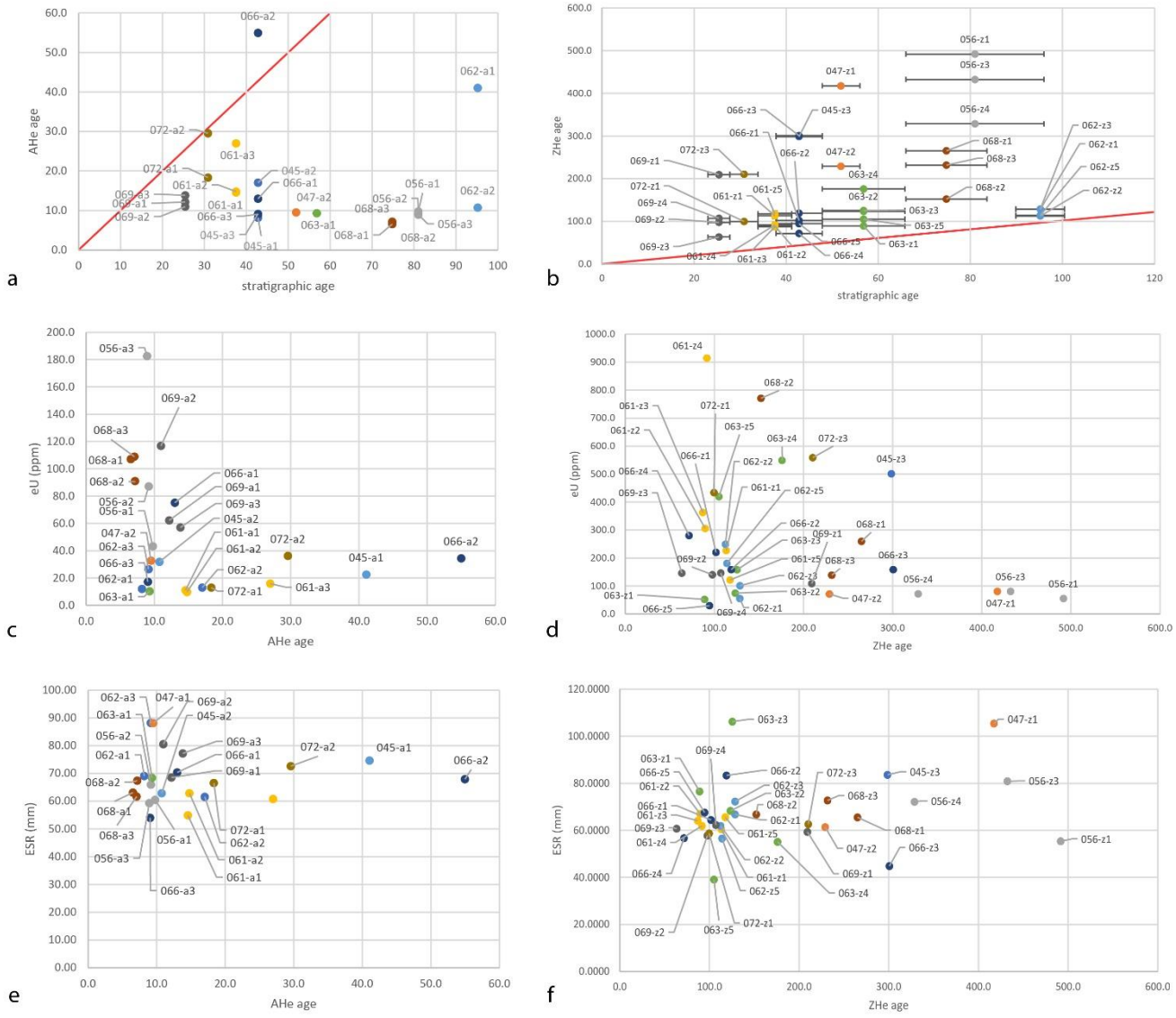

Figure A 1: Circle colour refer to a sample, the same colour code is applied for all graphs. a) Graphic of the AHe single grain age compared to the stratigraphic age. CAR19-066_a2 is the only non-reset grain. b) ZHe single grain age compared to the stratigraphic age. ZHe are non-reset and mark the sediment source age of exhumation. c) AHe single grain age as a function of eU (ppm) content. d) ZHe single grain age as a function of eU (ppm) content. e) AHe single-grain age as a function of ESR (equivalent sphere radius, in mm). f) ZHe single-grain age as a function of ESR.